Study of Structural and Optical Behaviour of Non-Stoichiometric Hexagonal $YMnO_3$

Thesis

Submitted to the

G. B. Pant University of Agriculture & Technology
Pantnagar-263145, Uttarakhand, INDIA

By

PRIYA MEHRA
B.Sc. (PCM)

IN PARTIAL FULFILMENT OF THE REQUIREMENTS

FOR THE DEGREE OF

Master of Science

(Physics)

July, 2018

ACKNOWLEDGEMENT

It's the solemn benediction of God who has given the opportunity to prepare this manuscript and provided me with strength and encouragement. I feel immense pleasure in expressing my sincere gratitude and profound sense of reverence to Dr. Gagan Dixit, Assistant Professor, Department of Physics and Chairman of my Advisory Committee for her inspiring guidance, untired co-operation, constant encouragement, constructive criticism and soothing affection during the course of investigation and preparation of this manuscript. I will be grateful to her forever, for the benefits of her guidance and moral teachings would be eternal.

I deem it to my privilege to acknowledge the indelible inspiration and continuous support received from the esteemed members of my advisory committee namely, Dr. Bhawana Pandey, Assistant Professor and Dr. Virendra Singh, Assistant Professor, Department of Physics I also express my sincere thanks to the honourable faculty members of Department of Physics for their love and cooperation with special regards to Dr. H.M. Agarwal(Ret. Professor and Head), Dr. U.C. Johri, Professor, Dr. R.C. Srivastava, Professor and Head of Department, Dr. Deepika P. Joshi, Assistant Professor, Dr. B.C. Chanyal, Assistant Professor, Department of Physics for their unending support and care.

I also feel great pleasure to acknowledge our Dean, College of Post Graduate Studies; Dean, College of Basic Sciences and Humanities, staff members of university library and K. N. Shukla Central Computing Facility.

I consider my privilege to thank all the teaching and non-teaching staff. The timely help provided by Mr. B. D. Joshi, Mr. R. S. Adhikari, and Mrs. Anuradha Shukla is unforgettable. I would also like to thank Munni Aunty and Mr. Gaurav for their help.

I am immensely indebted to Mr. Abhishek Pathak for his continuous help during the whole course of investigation.

I would like to thank Dr. Vivekananda, Associate Prof., Depatment of Chemistry for providing UV-Vis Spectroscopy facility. I am also thankful to Dr. J. P. Rai, Head of Deparatment, Department of Environmental Science for providing FTIR facility.

I also acknowledge the whole hearted cooperation received from my seniors Diksha Mam, Abhay Sir, Hem Sir, Shalini Mam, Dheeraj Sir, Saurbh Sir, Pramesh Sir, Raj Kumar Sir and Deepak Sir for their support and guidance. I am also thankfiul to Balwant Sir and Pankaj Sir for their valuable suggestions and discussions. Pleasant company and cooperation met by my batch-mates Kavita, Himanshu, Mayank, Rita, Harshita, Sukhwinder and my juniors are also acknowledged.

With the deep sense of gratitude and great pleasure, I express my regards and respect to my beloved parents Mrs. Sarita Mehra and Mr. Inder Singh Mehra for the abundant love they showered upon me without which I might not be able to pursue my consistence. I again bow my head before my parents' hardships, patience and perseverance because of which today I stand and that has kept me going at all hard times. I would like to express my heartfelt gratitude to all of my family members specialy who directly and indirectly provided me with all the help and moral support I ever needed.

I would specialy like to thank my loving brothers Vinod, Jitu bhaiya, Kartik, Karan, Tushar and Manu for their kind support and love in every part of my life. I would like to thank Laddu, Aaru and Nishu whose care, mischief and kind support did not ever let me feel out of my family and made my stay at Pantnagar memorable.

Lastly thanks to all beloved and respected people around me who directly and indirectly helped me during my degree programme and whose names could not be mentioned here.

July, 2018
Pantnagar

(Priya Mehra)
Authoress

CERTIFICATE

This is to certify that the thesis entitled **"Study of Structural and Optical Behaviour of Non-Stoichiometric Hexagonal $YMnO_3$",** submitted in partial fulfillment of requirements for the degree of **Master of Science** with major in **Physics** in the College of Post Graduate Studies, G.B. Pant University of Agriculture and Technology, Pantnagar, is a record of *bona-fide* research carried out by **Ms. Priya Mehra, Id. No. 51095**, under my supervision, and no part of this thesis has been submitted for any other degree or diploma.

The assistance and help received during the course of this investigation have been duly acknowledged.

Gagan Dixit

Pantnagar
July, 2018

(Gagan Dixit)
Chairman
Advisory Committee

CERTIFICATE

We, the undersigned members of the Advisory committee of **Ms. Priya Mehra, Id. No. 51095,** a candidate for the degree of **Master of Science** with major in **Physics**, agree that the thesis entitled **"Study of Structural and Optical Behaviour of Non-Stoichiometric Hexagonal $YMnO_3$"** may be submitted in partial fulfillment of the requirements for the degree.

(Gagan Dixit)
Chairman
Advisory Committee

(Bhawna Pandey)
Member

(Virendra Singh)
Member

CONTENTS

LIST OF TABLES

LIST OF FIGURES

Introduction

In modern world, the development of new generation devices has increased the demand of smart materials with multifunctional properties. Materials are being manipulated for modification of different properties. Multiferroics are special type of materials showing a number of different physical phenomenon that arise due to strong coupling between two or more ferroic order parameters. Due to multifunctionality these types of materials can be used in the field of telecommunications, microelectronics, computing, defense, aerospace, laser technology, microwave applications, transducer, actuators, computer memory, electo-optical modulator, light valves etc.

1.1 Multiferroic

It is believed that the term "multiferroic" was proposed by H. Schmid in the year 1994 (**H. Schmid, 1994**). Multiferroics are those materials which exhibit more than one type of ferroic ordering including electric, magnetic and elastic ordering. Magnetic ordering emerges due to interaction between magnetic dipoles. Electric ordering is due to ordering of local electric dipoles whereas elastic ordering is the result of ordering of atomic orbital due to strain. In multiferroic materials, an interesting and useful property occurs when magnetic-electric or magnetic-electric-elastic phase coexist. This effect is known as Magnetoelectric Effect (ME), **(Eerenstein *et al.* 2006).** In recent years, the term magnetoelectric has become popular as it facilitates the conversion between electric and magnetic field. When an external electric field is apllied, the magnetic properties of multiferroic compound changes, conversely when external magnetic field is applied it effects the electric polarization of that material. The overlap of ferroelectric and ferromagnetic materials representing multiferroic material is shown in Figure 1.1 (a) along with the relationship between magnetoelectric and multiferroic materials. Figure 1.1(b) shows multiferroic coupling effects.

1.1.1. Types of ferroics

Different types of Ferroic materials with their characteristics are shown in Figure 1.2 and discussed as follows:

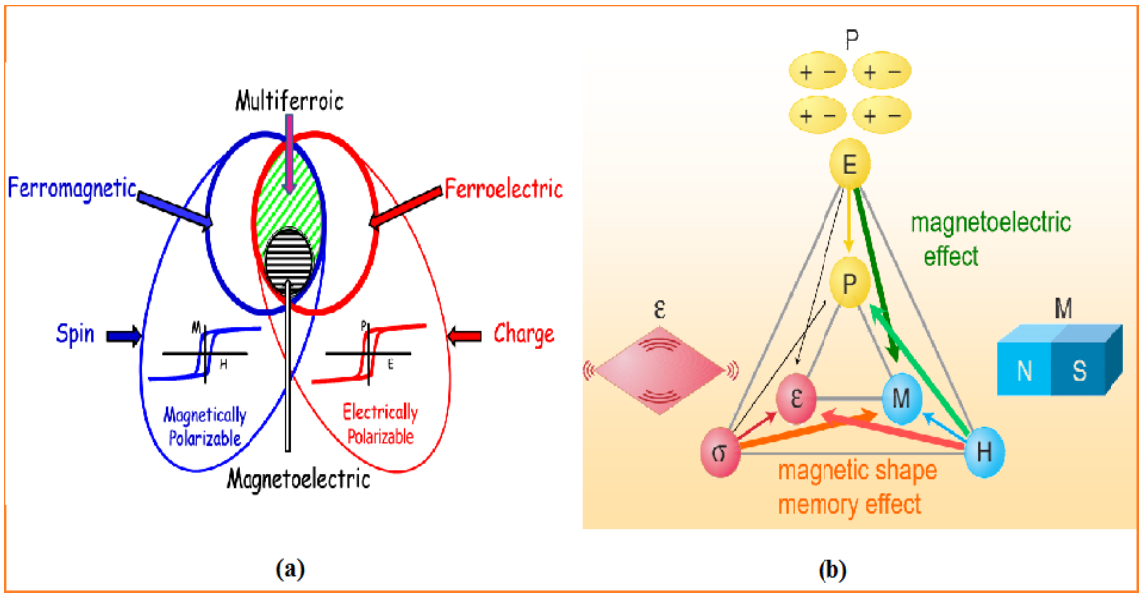

Figure 1.1: (a) Schematic illustration of the relationship between magnetoelectric and multiferroic materials and the requirement to be both (Eerenstein *et al.* 2006); (b) Schematic representation of possible coupling in multiferroic (Martin *et al.* 2008).

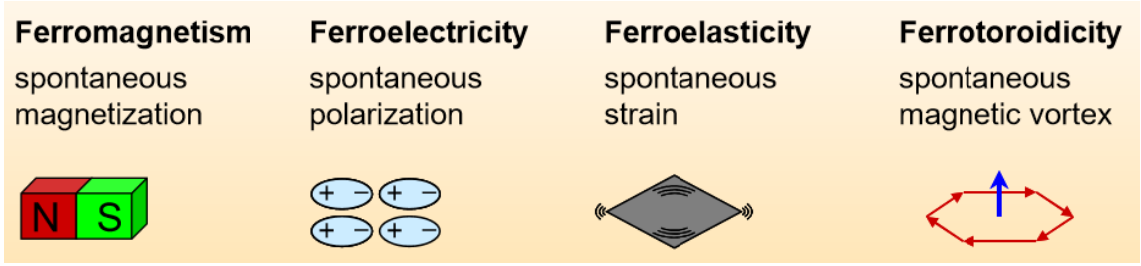

Figure 1.2: Primary ferroic properties of the material

1. **Ferroelectric –** Materials that have spontaneous electric polarization below an ordering temperature are called ferroelectric. The change in polarization is done by the application of applied electric field. Ferroelectric materials lack inversion of symmetry. Example- $BaTiO_3$

2. **Ferromagnetic**- Materials that exhibit spontaneous magnetic polarization in absence of external magnetic field. Example- Co, Fe

3. **Ferroelastic** - Materials that has spontaneous deformation and it can be switched hysterically by applied stress. Example- Nitinol (alloy of Ni & Ti)

4. **Ferrotoroidic-** Materials that has stable and spontaneous long range order parameter of microscopic magnetic torodial moments. The domains in ferrotoroidic material can be changed by an appropriate field, e.g. a magnetic curl. Example- $LiCo(PO4)_3$ and $Ba_2CoGe_2O_7$

Multiferroic materials have more than one ferroic ordering, so they can be of different types. On the basis of coupling of ferroic orders coexisting in them, following type of couplings between ferroic orders parameters are there **(Eerenstein *et al.* 2006):**

i. **Magnetoelectric coupling-** describes the effect of applied magnetic field on electric polarisation or vice versa.

ii. **Piezoelectricity** includes the effect of electric field on strain and the change in polarization when stress is applied.

iii. **Piezomagnetism** explains the change in strain with the application of magnetic field and the change in magnetization when stress is applied.

iv. **Electrostriction** describes that change in strain is a quadratic function of applied electric field.

v. **Magnetostriction** describes that change in strain is a quadratic function of applied magnetic field.

Present work will be focused on multiferroics having magnetoelectric coupling. Therefore now onwards, multiferroic means only magnetoelectric multiferroics.

1.1.2 Classification of Multiferroics

As discussed above, initially Magnetoelectric multiferroics were only those materials which have both ferromagnetism and ferroelecricity, but now the materials having any kind of magnetic ordering with electric ordering come under this category. The microscopic origin of ferromagnetism is generally same in all multiferroics, as it is due to partially filled d or f shells in rare earth ion or transition metals which create localized magnetic moment. The exchange interaction among these localized magnetic moment leads to magnetic ordering. But this is not so with ferroelectricity, the microscopic origin of ferroelectricty has different ways which lead to different type of multiferroic properties. In general, multiferroics are classified in two categories (**Khomskii, 2009).**

1.1.2.1 Type I multiferroics

These multiferroics are the materials in which ferroelectricity and magnetism originates by largely different mechanisms. Though the coupling in these multiferroics is quite low but their critical temperatures and spontaneous polarization values are high and this is the attractive feature of these types of multiferroics. For example bismuth ferrite ($BiFeO_3$) (T_N = 643 K, T_{FE} ~ 1100K, P ~ 90μC/cm^2). Depending upon the origin of ferroelectricity, type I multiferroics are further classified as follows:

(i) Multiferroic Pervoskites– The perovskites like $Pb(ZrTi)O_3$ or $BaTiO_3$ are best known multiferroics. Origin of ferroelectricity in such materials is because of the shift of the off-center transition metal ion as shown in Figure 1.3. These metal ions form strong covalent bonds with oxygens, through their d states which are not having any electron. On the other hand electrons present in d^n configurations produces magnetism in transition metals but reduces ferroelectric ordering in magnetic perovskites. Thus empty d sates are required for ferroelectricity and filled d states for magnetism.

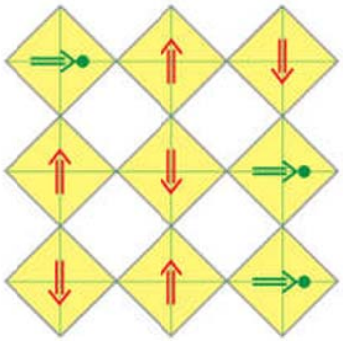

Figure 1.3: Green circles are ferroelectrically active d^0 ions, and the red arrows represent magnetic ordering. Ions with empty d states shift from the centers of O_6 octahedra represented by yellow region and thus lead to polarization shown by green arrows, coexisting with magnetic ordering.

(ii) Ferroelectricity due to lone pairs – In $BiFeO_3$, $PbVO_3$ etc. origin of ferroelectricity is due to Bi^{3+} and Pb^{2+} ions respectively. These ions have two outer 6s electrons. These two electrons do not form chemical bonds, so these are called lone pairs, or dangling bonds. They show high value of polarizability which is required for ferroelectricity according to classical mechanism. The origin of ferroelectricity or polarizability in these compounds can be explained on the basis of ordering of these lone pairs in one direction [Figure 1.4].

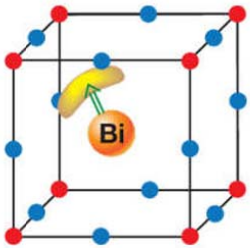

Figure 1.4: In materials like $BiFeO_3$ the ordering of lone pairs (yellow lobes) of Bi^{3+} contributes to the polarization (green arrow).

(iii) Multiferroics in which charge ordering causes ferroelectricity – Another mechanism leading to ferroelectricity is charge ordering. It is mostly observed in transition metal compounds, and mainly in those compounds which have transition metal ions of different valence state. If after charge ordering, both sites and bonds turn out to be inequivalent, this can lead to ferroelectricity (Figure 1.5). This mechanism is observed in systems like Nickelates ($RNiO_3$). Mostly this mechanism occurs for the systems in which there exist ions with different charge (mostly because they are different elements), or there occurs dimerization. For example: $TbMn_2O_5$ and Ca_3CoMnO_6. Next case is when site-centered charge ordering appears because structure of material is such as to have inequivalent bonds. For example in organic ferroelectric $(TMTTF)_2X$, and $LuFe_2O_4$.

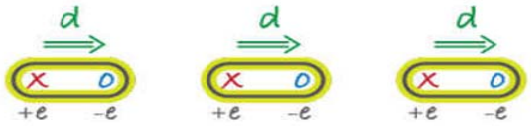

Figure 1.5: Coexistence of inequivalent sites with different charges showing charge ordered system in which inequivalent bonds, lead to ferroelectricity.

(iv) Geometric Ferroelectricity- This type of ferroelectricty is observed in ABO_3 type materials, where A and B are cations. Basically tilting of complex BO_5 polyhedra is responsible for ferroelectricity in these materials. For example $YMnO_3$ (Figure 1.6), where magnetic Mn^{3+} ions do nothing to cause ferroelectricity but the tilting of MnO_5 causes ferroelectricity. This tilting occurs to provide a closely packed structure, because of which oxygen ions shift towards Y ions.

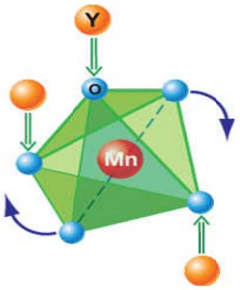

Figure 1.6: The tilting of MnO_5 block with a magnetic Mn ion at the center. It causes Y-O bonds to form dipoles (shown by green arrows), so that the system becomes ferroelectric

1.1.2.2 Type II multiferroic

The materials which show a particular type of ferroelectricity in their magnetically ordered state come under the category of Type II multiferroics. In these materials spin ordering breaks the inversion symmetry and produces a spontaneous polarization i.e. ferroelectricity. In these materials, electric and magnetic order parameters show very strong coupling, however the value of electric polarization in these materials is usually very small ($\sim 10-2\mu C/cm^2$). **Kimura *et al.* 2003** observed that magnetized $TbMnO_3$ show spontaneous polarization. After this, a number of other materials such as $Ni_3V_2O_8$, $MnWO_6$ have been found which show this type of polarization. Magnetic spin structure is responsible for magnetic ordering and it can be of any type either noncollinear (spiraling cycloid) or collinear. Both type of spin order can produce spontaneous polarization when they are placed on some specific lattice geometry. On the basis of mechanism of origin of ferroelectricity, type-II multiferroics can be divided into two groups: First one in which a magnetic spiral causes ferroelectricity and the others where ferroelectricity is due to collinear magnetic structures.

1.1.3 Four major crystallographic classes of multiferroics:

a. **Pervoskites –** $BaTiO_3$, $BiFeO_3$, $EuTiO_3$
b. **$BaMF_4$** where M = Mg, Co, Mn, Fe, Ni, Zn
c. **Boracites $M_3B_7O_{13}X$ –** where M is a divalent cation ranging from Cr to Ni and X is a halogen like Cl, Br and I. Ex- $Cr_3B_7O_{13}Cl$, $Ni_3B_7O_{13}I$
d. **Hexagonal magnetites $RMnO_3$ –** $YMnO_3$, $EuMnO_3$ & **Hexagonal Ortho Ferrites $RFeO_3$ -** $LuFeO_3$ **,** $DyFeO_3$

Out of these four classes**, Bismuth Ferrite (BFO)** is one of the earliest known and most studied multiferroic. It is an inorganic material having rhombhohedrally distorted structure. It is one of the few materials that show magnetic ordering as well as strong ferroelectricity at room temperature. For a long time it was thought not to be a promising material as it shows antiferromagnetic ordering. Later on it became the most studied multiferroic because of its high value of ferroelectric transition temperature (T_C = 1100 K) and Neel temperature (T_N = 650K). BFO is a pervoskite type of crystal in which ferroelectricity is caused by d^0 orbital whereas partially filled d^n orbital shows magnetic ordering. But there are certain limitations due to which it has restricted applications. Bismuth has high volatile nature due to which large numbers of oxygen vacancies are created in the compound. Multiple oxidation states of Fe generate high leakage current which reduces ferroelectricity in the BFO (**Makhdoom *et al.* 2012).** Antiferromagnetism in BFO is generated by its canted spin structure but it vanishes at macroscopic level because of the spiral spin structure of its magnetic domains **(Uniyal *et al.* 2008, Makhdoom *et al.* 2012).** Moreover, the pure synthesis of BFO is difficult **(Wang *et al.* 2003).** These limitations led researchers to study other multiferroic materials.

$RMnO_3$ Rare earth manganese oxides ($RMnO_3$) belong to class of multiferroic materials that have recently attracted a great deal of interest. These are very important for the application point of view in the field of magneto-electric sensors, spintronics and even in the green energy devices for the reduction of power consumption **(Mori *et al.* 2005, Han *et al.* 2013**, **Raneesh *et al.* 2013).** Many studies have been done and still going on these rare earth magnetites as they show a lot of interesting properties like colossal magneto resistance (CMR), giant capacitance, geometric ferroelectricity, Zener double exchange, orbital ordering, half metalicity, Polaronic effect and Jahn Teller effect and so on (**Helmholt *et al.* 1993 and Jin *et al.* 1994**) Magnetites are the ions where the oxygen (O) ions are connected with manganese (Mn) ions and the rare earth ions are presented in the gap of Mn and O ions. Rare earth magnetites also show high value of magnetoelectric coupling. Its unrevealed properties and its complex structure make these materials important to be explored.

Rare earth magnetites (R= yttirium and other rare earth metals) show crystallization in two structural phases **(Yakel *et al.* 1963).** The rare earth metals which have smaller radius like Ho, Er, Tm, Yb, Lu, and Y crystallizes in hexagonal phase and have $P6_3cm$ space group whereas metals having larger radius such as La, Pr, Nd, Sm, Eu, Gd, and Tb have a distorted orthorhombic perovskite structure and Pnma space group

(Yakel *et al.* 1963 and Fiebig *et al.* 2002). It was observed that both hexagonal and orthorhombic manganites show some kind of Magnetic ordering but electric ordering or ferroelectricity is shown by hexagonal manganites only. Therefore, the hexagonal yttrium and rare-earth manganites also called as ferroelectromagnets are supposed to be more interesting for studying. Now recent studies show that orthorhombic $YMnO_3$ also show ferroelectricity and belong to Type II multiferroics, in which electromagnetic coupling is strong but the value of electric polarization is small.

Orthoferrites ($RFeO_3$) is another important class of multiferroics. Structure of orthoferrites is similar to that of hexagonal rare earth manganites. The only difference is that orthoferrites have Fe^{3+} ions in place of Mn^{3+} ions,and because of this Orthoferrites show weak ferromagnetism unlike antiferromagnetism shown by rare earth manganites.

Present thesis work is focused on the study of hexagonal $YMnO_3$.

1.1.4 $YMnO_3$

Yttrium is not a rare earth element yet yttrium manganite ($YMnO_3$) is considered in the $RMnO_3$ family. There are many reasons which support the consideration of $YMnO_3$ in the $RMnO_3$ family. Firstly, structure wise it is very similar to hexagonal rare earth magnetites (h-$RMnO_3$) compounds (R = Ho – Lu). Despite its stable phase in hexagonal form it also shows orthorhombic structure. Secondly, $YMnO_3$ behaves similar to $RMnO_3$ in both the phases.

Study of hexagonal $YMnO_3$ (h-YMO) is important because it is a multiferroic material having ferroelectric phase along with antiferromagnetic ordering .Yttrium manganite is an improper ferroelectric (whose primary order parameter is not polarization but another physical quantity such as magnetization) (**Kim *et al.* 2000**). Ferroelectric transition temperature i.e. Curie temperature for h-$YMnO_3$ is quite high (Tc~900 K) and antiferromagnetic transition temperature i.e. Neel Temperature is low (T_N ~70 K) **(Van Aken *et al.* 2004).** In h-YMO, Y^{3+} ion separates the trigonal bipyramidal MnO_5 ion which is linked with two apical and three in-plane oxygen ions as shown in Figure 1.7. On comparing the ferroelectric and paraelectric crystal of YMO it is seen that in paraelectric structure the layer of Y^{3+} ion separates the layer of MnO_5 ion whereas in the ferroelectric crystal there is buckling in yttrium layer as well as tilting of MnO_5 ions **(Vajk *et al.* 2005; Fennie and Rabe, 2005)** and this buckling and tilting is responsible for the origin of ferroelectricty in $YMnO_3$ (YMO).

The ABO_3 oxide compounds mainly crystallize into a simple perovskite structure. The structure of ideal pervoskite is cubic in nature with Pm3m space group. The stability condition of the pervoskite structure depends on the Goldschmidt tolerance factor t:

$$t = \frac{R_A + R_O}{R_B\sqrt{2} + R_O}$$

where R_B, R_A and R_O are the ionic radii of B, A and O atoms in the ABO_3 structure respectively. . The tolerance factor of YMO is t < 1 means the A atom is too small for the structure and cannot effectively bond with neighboring O atoms. This leads to the unstability in the compound and it causes geometrical frustration in compound. The compounds having t < 1 stablizes in hexagonal structur. The buckling in trigonal bipyramidal MnO_5, with the displacement of Y ions leads to ferroelectricity in the compound **(Van Aken *et al.* 2004**). The origin of antiferromagnetism in YMO is due to the Mn ions. In YMO, the angle Mn-O-Mn is close to 180°, facilitating magnetic ordering by an indirect exchange interaction between the Mn ions through the O ions **(Huang *et al.* 1997**). . YMO shows G type antiferromagnetism (both intra and inter order coupling are antiferromagnetic in nature).

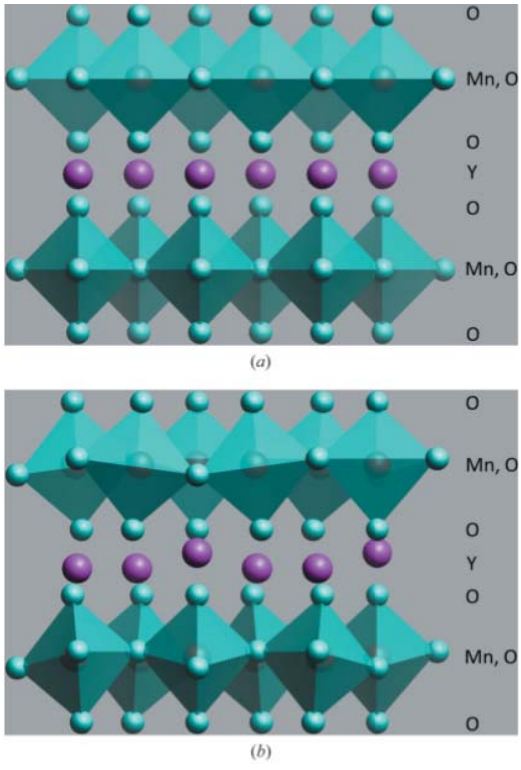

Figure 1.7: Crystal structure of $YMnO_3$; a) the paraelectric phase at high temperature b) the ferroelectric phase at room temperature (Adapted from Ref. Gibbs *et al.* 2011)

1.1.5 THESIS OUTLINE

For understanding the mechanism of coupling between magnetism and ferroelectricity in hexagonal-YMO, information about the electronic as well as magnetic behavior of the material must be known. A lot of work is done to understand the magnetic behavior of YMO but its electronic structure is still not completely known and electronic structure can be revealed by optical spectroscopy. Therefore, present work is focused to study the effect of composition of YMO on its structural and optical properties. The whole work of this thesis is divided into five chapters. First chapter gives the introduction about the multiferroics and in particular hexagonal rare earth magnetites, its importance and use in various fields. The second chapter deals with the review of earlier work done on this material and its use in the present work. Third chapter tells about the methods and the techniques used for the synthesis and characterization of samples. Fourth chapter contains the results and analysis of the experimental work done. Fifth chapter gives the summary and conclusion of the present work done.

Review of Literature

A series of rare earth magnetites $RMnO_3$ of different composition were studied theoretically and experimentally by several researchers. $YMnO_3$ got attention because of its interesting electric and magnetic properties. A brief review is given for the previous work done on this system is given below:

Yakel *et al.* 1963 investigated the crystal structure of heavy Lanthanides (holmium, erbium, thulium, ytterbium and lutetium) and Yttrium and showed that the compounds have hexagonal structure and belong to $P6_3cm$ space group. The crystal structure has five and seven fold coordinated polyhedral about manganese and rare earth ions. Trimerization of Mn ions was found to be the reason for stability of distorted pervoksite structure.

Huang *et al.* 1997 investigated the coupling between the ferroelectric and antiferromagnetic orders in $YMnO_3$. Anomalies in the dielectric constant and loss tangent near Neel temperature confirmed about the coupling between the ferroelectric and antiferromagnetic order in this compound.

Degenhardt *et al.* 2001 studied the electronic structure of rare-earth manganites $RMnO_3$ (R = Sc, Er, Tm, Yb, Y, Ho, Lu) by Second harmonic (SH) spectroscopy. They found strong absorptions at 1.3 eV at 300 K and 1.5 eV at 4 K. This peak was due to the spin-allowed $5\Gamma1$ *(5Γ1)* $\rightarrow$ $5\Gamma1$ *(5Γ5)* transitions within the t_{2g} and e_g orbitals of Mn^{3+} ($3d^4$) ions splitted by the local crystalline field.

Kalashinkova *et al.* 2003 discussed about electronic and optical properties of hexagonal $YMnO_3$ by using the ellipsometry technique in the spectral range of 0.7–5.4 eV. The electronic structure of hexagonal magnetite was found to differ from that of orthogonal magnetite. Presence of intense electric dipole absorption band at about 1.6 eV corresponds to charge transfer from the oxygen band to the lower manganese subband.

The nature of the ferroelectric transition in YMO was studied by **Van Aken *et al.* 2004** using first-principles DFT calculations. The ferroelectric phase was induced by buckling of the trigonal bipyramidal MnO_5 polyhedra, supported by displacements of the Y ions, which leads to net electric polarization in the compound. Oxygen rotations and long-range dipole–dipole interactions both cooperate to drive the system towards the

stable ferroelectric state. The polarization was due to the unusual Y-site coordination and the triangular and layered MnO_5 network.

Kang *et al.* 2005 studied the electronic structure of YMO by resonance photoemission spectroscopy and found the absorption peak at 7eV. They concluded that $YMnO_3$ is a charge-transfer insulator.

Choi *et al.* 2008 investigated the electronic structure and optical properties of thin films of $RMnO_3$ (R= rare earth magnetite) by temperature-dependent transmission spectroscopy. The optical absorption peak was found at nearly 1.7eV. The temperature and magnetic field dependent measurements have shown strong coupling between electronic and magnetic structure in multiferroic oxide system.

Nanocrystals of $YMnO_3$ were synthesized by **Wang *et al.* 2011** by polyacrylamide gel route. The optical bandgap of $YMnO_3$ samples were determined by optical absorption and it was observed that decrement in crystallite size lead to increment in energy band gap because of quantum size effect.

Raneesh *et al.* 2013 synthesized the crystalline YMO by sol gel route. γ rays were subjected on YMO samples and the changes in surface morphology were observed. It was found that the multiferroic properties of YMO degraded after employing γ radiation.

Ahmad *et al.* 2015 prepared $YMnO_3$ nanocrystals (nearly 48 nm) by low temperature polymeric citrate precursor route. The optical band gap was found to be 3.7 eV by UV-Vis Spectroscopy. The Photoluminescence spectra show the compound is a wide-band gap semiconductor.

Lima *et al.* 2017 investigated optical absorption (OA) spectrum and electronic structure of the hexagonal $YMnO_3$ with the help of first principal calculations based on DFT. It was reported that experimental OA spectrum of the $YMnO_3$ can be reproduced satisfactorily only if low-temperature noncollinear magnetic order is considered.

2.1 Effect of doping on Yttrium Magnetite:

A large number of reports have described the changes in structural, optical and magnetic behavior of $YMnO_3$ by doping foreign element. Here is a brief report on the effect of doping on YMO:

Asaka *et al.* 2005 reported that there is a change in phase from hexagonal to rhombohedral structure when Ti is doped at Mn site in $YMnO_3$. This is due to weakly trimerized Mn(Ti)O layers.

Sekhar *et al.* 2003 studied doping effects of Er on $YMnO_3$ and found that Er doping at the Y site of $YMnO_3$ significantly modifies the geometrical frustration effects of the Mn moments with a triangular spin structure which affects the magnetic structure of $YMnO_3$.

Yoo *et al.* 2012 investigated magnetic and structural properties of $YMn_{1-x}Cr_xO_3$ with x= 0, 0.05, and 0.1, prepared by solid-state reaction route. It was observed that Cr-doped samples exhibit increase of the ferromagnetic transition temperature which attributed to double-exchange interaction between Cr^{3+} and Mn^{3+} ions.

Zhang *et al.* 2013 studied the change in magnetization and spin frustration factor when Al is doped at Mn site in $YMnO_3$ and increase in magnetization and decrease in frustration factor was observed. The antiferromagnetic transition temperature was found to decrease as the doping content increases in the sample.

Chauhan *et al.* 2014 studied the effect of Gd substitution at Y site on the structural, magnetic and dielectric properties of Yttrium Magnetite. Nanoparticles of $Y_{1-x}Gd_xMnO_3$ (x=0, 0.05) were prepared by solid state reaction method. It was reported that the value of lattice parameter 'a' decreased and 'c' increased with Gd substitution. The antiferromagnetic transition temperature (T_N) was increased up to 88K due to change in Mn-Mn distance. Dielectric constant of the sample was also increased due to change in tilting of MnO_5 trigonal bipyramids.

Rathod *et al.* 2016 have found that the dielectric constant and Ac conductivity values were increased in Zr doped h-$YMnO_3$ due to its disordered structure and ionic mismatch.

Dai *et al.* 2016 investigated the effect of doping of Ru on propeties of $YMnO_3$. The unit-cell volumes and lattice parameter 'a', 'c', of all doped samples were increased because of the larger radius of Ru^{3+}. Weak ferromagnetic (FM) ordering was strengthened while the antiferromagnetic (AFM) interaction was suppressed by increasing Ru^{3+} dopant content. The increased FM interaction was ascribed to the modification of Mn-Mn bond distance and weakened of trimerization of Mn ions.

Muneeshwaran *et al.* 2017 synthesized Dy doped $YMnO_3$ samples by soft chemical co-precipitation technique. A weak ferromagnetism was observed in the samples which were found to decrease with increase in Dy concentration.

2.2 Non- stoichiometric YMO:

Above mentioned report confirms that the properties of YMO can be modified effectively by chosing suitable dopants. However, there are some reports where modification in properties of YMO was achieved just by changing the stoichiometry of the compound.

The transport properties of domain walls in oxygen deficient multiferroic $YMnO_3$ single crystals were studied by **Du *et al.* 2011** using piezoresponse force microscopy and atomic force microscopy. It was observed that thermal activation of Oxygen vacancies results in changing the local band structure of the molecule due to which the conductance of domain wall's (DWs) had increased.

Gerald *et al.* 2011 investigated non-stoichiometry effects on the hexagonal structure of $REMnO_3$ (RE = Er, Dy).In RE excess films secondary phase of RE_2O_3 were formed whereas in Mn excess films no secondary phase was observed. A linear decrese of lattice parameter was found when RE/Mn ratio was less than 1.

Daborwoski *et al.* 2011 synthesized off stoichiometric $Dy_{1-x}Y_xMnO_{3+\delta}$ samples by solid state reaction method. It was found that changes in oxygen content were related to alternation of Mn coordination to oxygen. $Dy_{1-x}Y_xMnO_{3+\delta}$ samples absorb oxygen in large amount and rapidly release it during transition back to stoichiometric samples. Due to its large oxygen storage capability $Dy_{1-x}Y_xMnO_{3+\delta}$ has many advantages over other materials for example, the lowest cycling temperatures, nontoxicity, low cost and thermodynamical stability.

Chen *et al.* 2012 investigated the structural, ferroelectric, and magnetic interaction between oxygen vacancies and domain structures of $YMnO_3$ crystal. Neel temperature (T_N) and magnetization of the compound were found to be lower than the stoichiometric $YMnO_3$ which is attributed to the location of structural distortion at domain wall's (DWs) induced by oxygen vacancies.

Abugyada et al. 2015 synthesized stoichiometric $RMnO_{3+\delta}$ (R = Er, Y, and Ho) through solid state reaction method. It was found that $RMnO_{3+\delta}$ have reversible oxygen storage capability means sharp inclusion and exclusion of interstitial oxygen at accessible temperature. This had increased their functionality in generation of oxygen rich gases and in extraction of oxygen from air for industrial applications.

Cheng *et al.* 2015 studied the correlation between Oxygen vacancies and Mn ion sites. It was found that the in-plane oxygen (O_P) vacancies caused the off-centered shift and in plane movements of Mn ions.

Cheng *et al.* 2016 investigated the influence of oxygen vacancies (VO) on the magnetic properties of $YMnO_3$. It was observed that the structures with axial oxygen vacancies can nduce nonzero net magnetization along *c* -axis, i.e. ferromagnetism along the *c* -axis.

Motivation for Present Work:

From literature review, it observed that A-site substitution of Y ion and B-site substitution of Mn ion can effectively modulate the local microstructures and physical properties of materials. It becomes complicated to study the effect of extra element as dopant because it may affect the microstructure of parent material. Researchers have also modified the properties of YMO by self doping or by not having any foreign dopant or by changing the stoichiometry of samples and the studies have shown fruitful results as discussed above. Non-stoichiometric YMO/$RMnO_3$ is being studied for oxygen storage also. Since most of the work in non- stoichiometric YMO was focused on electric and magnetic behavior only and no studies have been done to study the effect of change in Y, Mn or O on optical properties, present work is motivated for this study. Also, the optical studies will help to understand the electronic structure of the materials. So the objective of this thesis is to study the optical and structural properties of non-stoichiometric YMO having different concentrations of Y, Mn and O atoms.

Materials and Methods

Present thesis work is focused to study the structural, morphological and optical properties of the samples using X-Ray Diffraction, Fourier Transform Infrared Spectroscoy, Scanning Electron Microscopy, Energy Dispersive X-ray spectroscopy and UV-vis spectroscopy. In this chapter basic principle of operation of the techniques used for the synthesis and characterization of samples is discussed.

3.1 Synthesis of Yttrium Magnetite

Solid State reaction Method:

Presently, non stoichiometric (Y deficient, Mn deficient and Mn excess) samples of hexagonal $YMnO_3$ were synthesized by solid state reaction method. For this, Y_2O_3 and MnO_2 powders were weighed corresponding to the compositions $Y_{0.95}MnO_3$, $YMn_{0.95}O_3$, $YMn_{1.05}O_3$ respectively. The powders were then mixed manually in pestle and mortar and grounded for 6h. After homogeneous mixing of the reagents the powders were pressed into pellets by applying a pressure of 5 Ton. Then the pellets were calcined in furnace at 1200°C for 13 hours, using Alumina Crucibles. The decomposition of the mixed powder by heating below its melting point is known as calcinations. After calcination the pellets were sintered at 1300°C for 13 h. Sintering is the process of heating at relatively higher temperature and for longer duration than used during calcinations. Following reaction takes place for the synthesis of compounds of $YMnO_3$:

$$\mathbf{2Y_2O_3 + 4MnO_2 \rightarrow 4YMnO_3 + O_2}$$

After synthesis the pellets were characterised for the confirmation of structure, phase and composition.

3.2 Structural & Phase Characterisation:

3.2.1 XRD

XRD is an analytical method for structural and phase characterization of materials. It was first introduced by Von Laue in 1912. X−ray diffractometer consists of three basic parts: X−ray tube, Sample holder and X−ray detector.

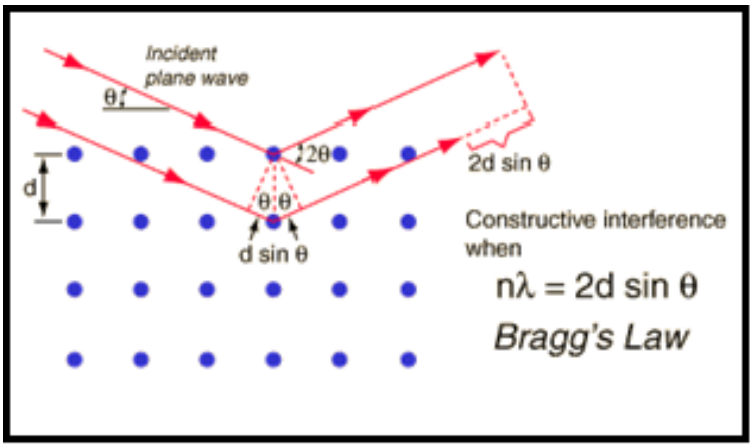

Figure 3.1: Bragg's law

X-ray tube has a cathode ray tube in which filament is heated to produce highly charged electrons. These electrons are accelerated by suitable voltage and are made to hit the target placed in X-ray tube. In this process, electrons loose energy in the form of X-rays. Collimated X−rays coming out of the X-ray tube are incident directly on the sample. The intensity of the reflected X−rays is recorded by rotating the sample and detector. When the geometry of the incident X−rays impinging the sample satisfies the Bragg Equation, constructive interference occurs for the x-ray scattered from the successive atomic planes formed by the crystal lattice of the material (Figure 3.1) and a peak in intensity occurs. Bragg's equation is given by:

$$\mathbf{2dsin\theta = n\lambda} \qquad (3.1)$$

where d is the interplanar spacing, θ is the angle of diffraction, n is the order of diffraction, λ is wavelength of X-rays.

A detector records and processes this X−ray signal and converts the signal to a count rate which is then output to a device such as a printer or computer monitor. The intensity of diffracted X−rays is continuously recorded as the sample and detector rotate through their respective angles (θ). Results are presented as peak positions at 2θ and X−ray counts (intensity) in the form of a table. Figure 3.2 shows the schematic representation of X-ray Spectrophotometer. Presently, Siemens D-5000 X-ray Diffractometer shown in Figure 3.3 was utilized to collect X-ray diffraction data at 40 kV, 40 mA for Cu Kα with a wavelength of 1.5406 Å.

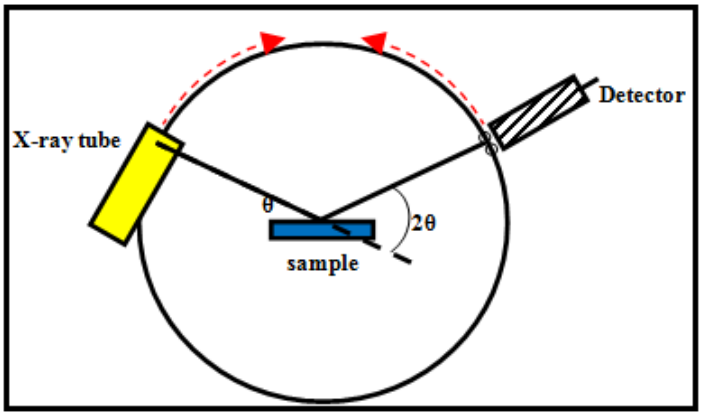

Figure 3.2: Schematic Diagram Of X-ray Spectrophotometer

Figure 3.3: X-ray Spectrophotometer

From XRD pattern various parameters can be estimated in the following way:

a) Crystallite size

The crystallite size (S) was calculated from XRD data by using Scherrer's formula (**Gagan *et al.* 2013**).

$$S = \frac{K\lambda}{B\cos\theta} \qquad (3.2)$$

where, B is full width at half maximum. K is a constant that depends on the shape of crystallites and has the value $2(\ln 2 / \pi)^{1/2} = 0.93$.

b) Lattice parameter

The lattice parameter was determined by the equation:

$$\frac{1}{d^2} = \frac{4}{3}\left(\frac{h^2+k^2+l^2}{a^2}\right) + \frac{l^2}{c^2} \quad (3.3)$$

On solving the equation for (h,k,l) (110) and (400) respectively we get:

$$a = \frac{\lambda}{sin\theta_1} \quad \text{and} \quad c = \frac{\lambda}{2sin\theta_2} \quad (3.4)$$

where, θ_1 is the peak position for (110) and θ_2 is the peak position for (400), h, k, l are the Miller indices, λ is the wavelength of radiation used and θ is diffraction angle.

3.2.2 Fourier Transform Infrared Spectroscopy (FTIR)

Infrared spectroscopy is an important analytical technique used to identify the presence of functional groups in a molecule. It can also be used to identify pure compound or to detect the impurity in pure compound. When a sample is placed in infrared radiation the molecule will absorb only those radiations which have energy corresponding to the frequencies of their vibrational modes and the other radiations will be transmitted. The transmitted light is measured by an infrared spectrometer and the missing radiation informs about vibrational structure of molecule. Since each molecule has different structure, therefore has different vibrational modes and different IR spectrum. In this way IR spectroscopy helps in identification of molecules. Original infrared instruments were having drawback of slow scanning process. A solution was developed in the form of an interferometer that helps measuring the signal very quickly. The resulting signal is converted into frequency spectrum by a well-known mathematical technique called Fourier transformation. Therefore, the resulting spectrum is called FTIR spectrum and IR spectroscopy as FTIR spectroscopy. The basic components of an FTIR spectrometer are**:** The Source that emits light in infrared region, the Interferometer for spectral encoding,Sample holder to place the sample, Detector to detect transmitted beam and the Computer, where Fourier transformation takes place and final infrared spectrum is displayed on the screen. Presently, Bruker Alpha II model shown in Figure 3.4 was used to record the spectra in the range of 490 cm^{-1} to 4400 cm^{-1}.

Figure 3.4: FTIR spectrometer

3.3 Scanning Electron Microscopy /Energy Dispersive Spectroscopy

SEM is used to study the morphology of the samples. It is equipped with a cathode and magnetic lenses to create and focus a beam of electrons. These electrons when strike the sample surface produces secondary electrons (SE), back scattered electrons (BSE) and X-rays. SE are used to produce high resolution images of the sample surface and BSE and X-rays for detection of composition of sample. When high energy beam of charged particle hits the sample the electron in the inner shell of the atom get excited. These excited electrons create vacancy in the shell and the electron from higher energy shell occupies that space and an amount of energy is released. The energy is released in the form of characteristic X-rays and is equal to the difference in energy between higher and lower shell as shown in Figure 3.5. Since each atom has it's unique energy levels therefore emitted X-rays are also unique and helps to indentify the atom. Energy dispersive spectrometer measures the number and energy of the X−rays emitted from the sample. Experimental arrangement of Energy dispersive X-ray Spectroscopy (EDAX/EDX/EDS) consists of four primary components: Beam source, X−ray detector, Pulse processor and Analyzer. EDX systems are most commonly found on scanning electron microscopes (SEM). The EDX X−ray detector (lithium drifted silicon) measures the relative abundance of emitted X−rays versus their energy. A charge pulse is created when X-ray strikes the detector. This charge pulse is proportional to the energy of X−ray. Charge−sensitive preamplifier converts this charge pulse into voltage pulse. Multichannel analyzer sorts the voltage pulse and sent it to computer for display and further data evaluation.

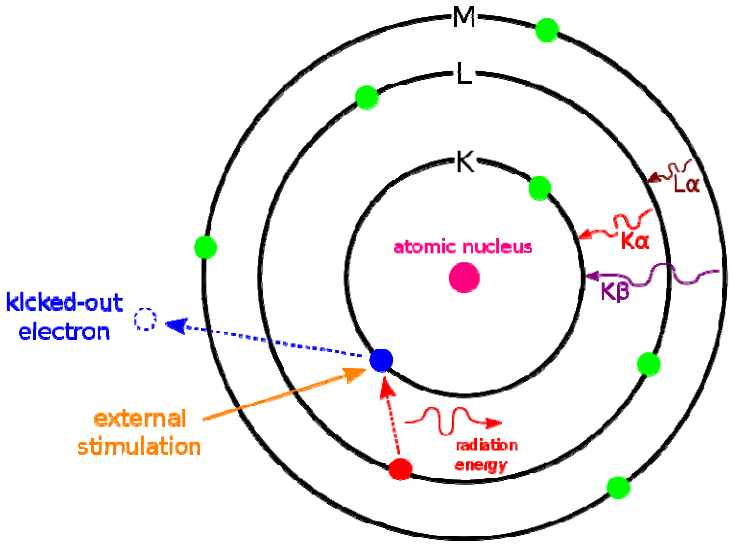

Figure 3.5: Principle of EDX

Figure 3.6: EDX Spectrometer

Presently, Morphology of the samples was recorded using a Scanning Electron Microscope (SEM; FEI Inspect-F, USA) operating at an accelerating voltage of 10 kV and a working distance of 15.4 mm. The elemental composition was obtained by an Energy Dispersive X-ray Spectrometer (EDS; JEOL JSM-6330F, JEOL, Japan) using a

current of 10.5 μA, a potential of 15 kV, and a working distance of 15 mm. Figure 3.6 shows a typical SEM/EDS machine.

3.4 UV−Vis Spectroscopy

The spectroscopy which uses photons of visible and its adjacent ranges is called UV-Vis Spectroscopy or electronic spectroscopy. Absorption of light by molecule results in electronic as well as rotational and vibrational transitions in a molecule. The amount of light transmitted (I) through a sample absorbing UV or visible light is often expressed as Beer-Lambert's law, given by:

$$\mathbf{I = I_0}\, e^{-\epsilon_\lambda C x} \tag{3.5}$$

where I_0 is the incident light intensity, C is the concentration of the sample, ε_λ is the molar absorptivity and x is the path length of the light traverses through the sample. The above equation can be written as:

$$\frac{\mathbf{I}}{\mathbf{I_0}} = \mathbf{e^{-\alpha x}} \tag{3.6}$$

where α is the absorption coefficient of the sample and can be written as a product of molar absorptivity and the concentration of absorbing species. The absorbance is:

$$\mathbf{A = - \log (I/Io)}$$

UV-Vis absorption spectrum is a plot between absorbance A and wavelength λ (or energy hv). Positions of absorption peaks give a measure of band gap of the sample or electronic transition.

Experimental Set up of UV- Vis Spectrophotometer consists of a light source (which emit light in UV- Vis region), a monochromator, sample holder (cuvettes), a detector, signal processor and readout. The light source (tungsten lamp, xenon arc lamp etc.) emits light which after passing from monochromator splits up into two equal intensity beams. One of the light beam passes through cuvettte (quartz or glass) containing sample which is being studied and the other one passes through reference (solvent). After passing from cuvettes the intensity of the transmitted lights is measured by electronic detectors and compared with that coming from the reference. This informs

about the light absorbed by the sample (absorbance). Then it displays the information on screen. Figure 3.7 shows schematic diagram of UV-Vis spectrophotometer.

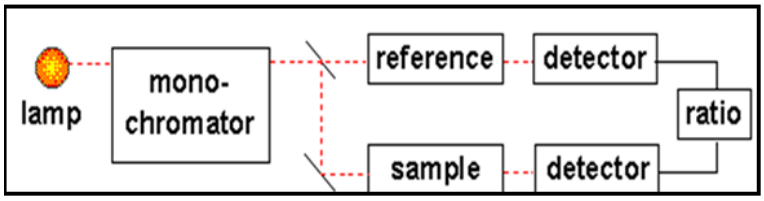

Figure 3.7: Schematic representation of UV-Vis Spectrophotometer

Presently, Genesys 10s UV−Vis−NIR Spectrometer, shown in Figure 3.8 having Xenon Flash Lamps was used. The wavelength Range of the spectrometer was 190 nm-1100 nm, but the spectrum was recorded in 200-800 nm range in absorbance mode with a Scan Speed of 4200 nm/min.

Figure 3.8: UV-Vis Spectrophotometer

Results and Discussion

Results obtained from X-Ray Diffraction, Energy Dispersive Spectroscopy, Fourier Transform Infra red and UV-visible Spectroscopy for YMO samples having different stoichiometry, are presented in this chapter. All results are discussed in terms of the concentration of Y, Mn and O ions in the samples, and an attempt has been made to correlate the stoichiometry with the structural and optical behavior the YMO samples.

4.1 SEM/EDS

SEM images of representative samples A, D, H and I are shown in Figure 4.1. The images were taken at a resolution of 5 μm for A and 50 μm for rest of the samples G, H, I. The images revealed that the surfaces of samples are smooth and dense. Atomic percentage of Y, Mn and O corresponding to each sample is shown in Figure 4.2. The atomic percentage is estimated from the EDS spectra shown in Figure 4.3. No element other than Manganese, Yttrium and Oxygen was detected in any of the samples. In Figure 4.4, samples are arranged corresponding to ascending order of Y/Mn ratio. On the basis of atomic percentage the structural formula is calculated for all samples and listed in Table 4.1.

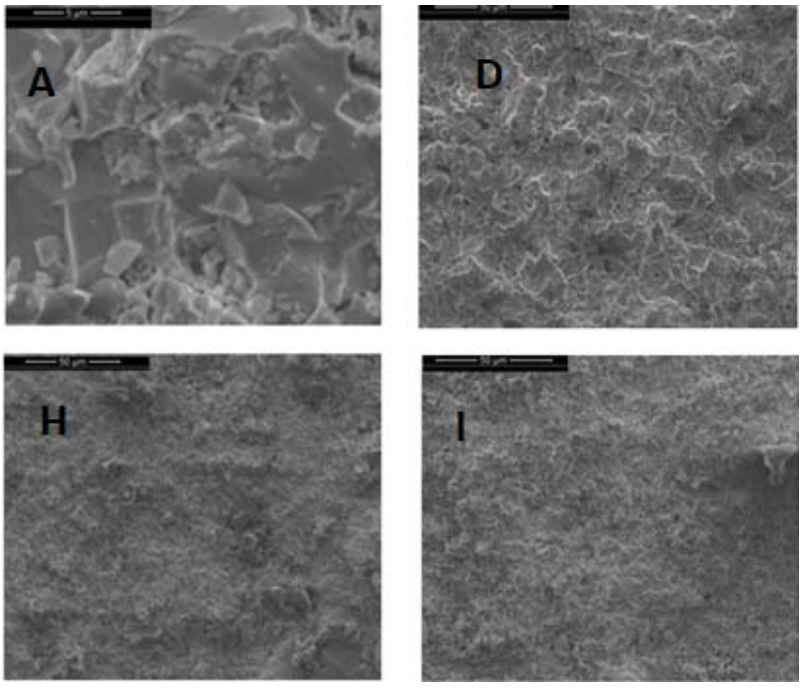

Figure 4.1: SEM images of samples A, D, H, I

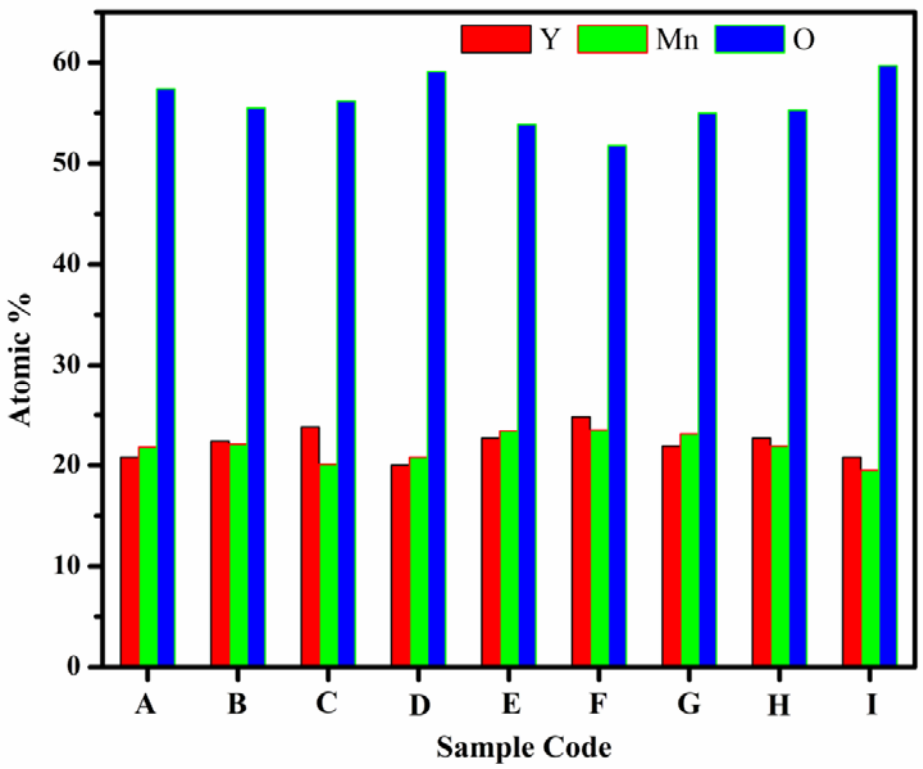

Figure 4.2: Variation of atomic percentage of Y, Mn and O with respect to sample code

Table 4.1: Structural formula for all YMO samples

Sample Codes	Compositions	Y/Mn ratio
A	$Y_{1.04}Mn_{1.04}O_{2.87}$	0.954
B	$Y_{1.12}Mn_{1.11}O_{2.78}$	1.013
C	$Y_{1.19}Mn_{1.001}O_{2.81}$	1.184
D	$Y_{1}Mn_{1.04}O_{2.96}$	0.961
E	$Y_{1.14}Mn_{1.17}O_{2.70}$	0.971
F	$Y_{1.24}Mn_{1.18}O_{2.59}$	1.055
G	$Y_{1.1}Mn_{1.16}O_{2.75}$	0.948
H	$Y_{1.14}Mn_{1.1}O_{2.76}$	1.036
I	$Y_{1.04}Mn_{0.98}O_{2.99}$	1.066

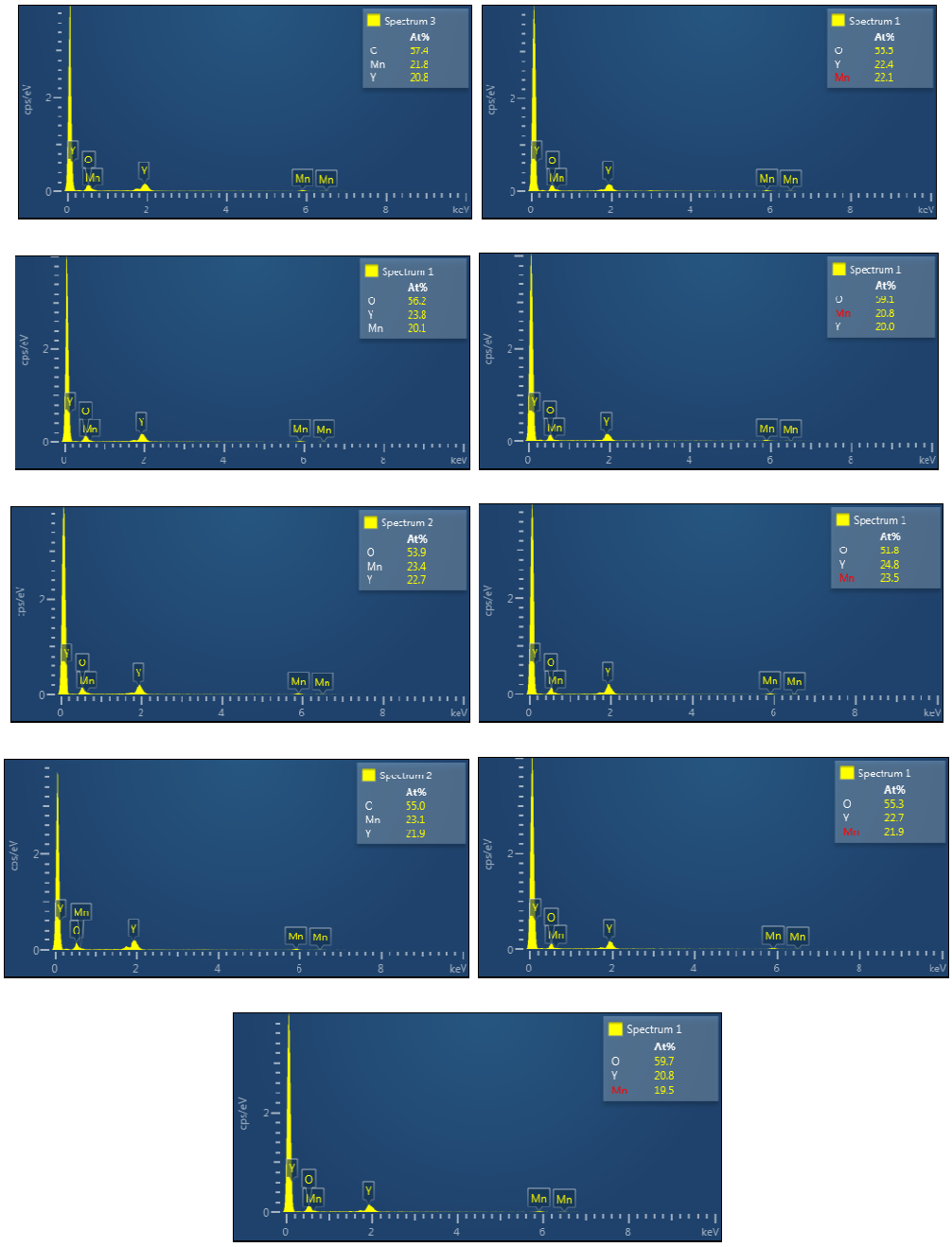

Figure 4.3: EDS spectra for all samples A, B,C,D,E,F,G,H,I

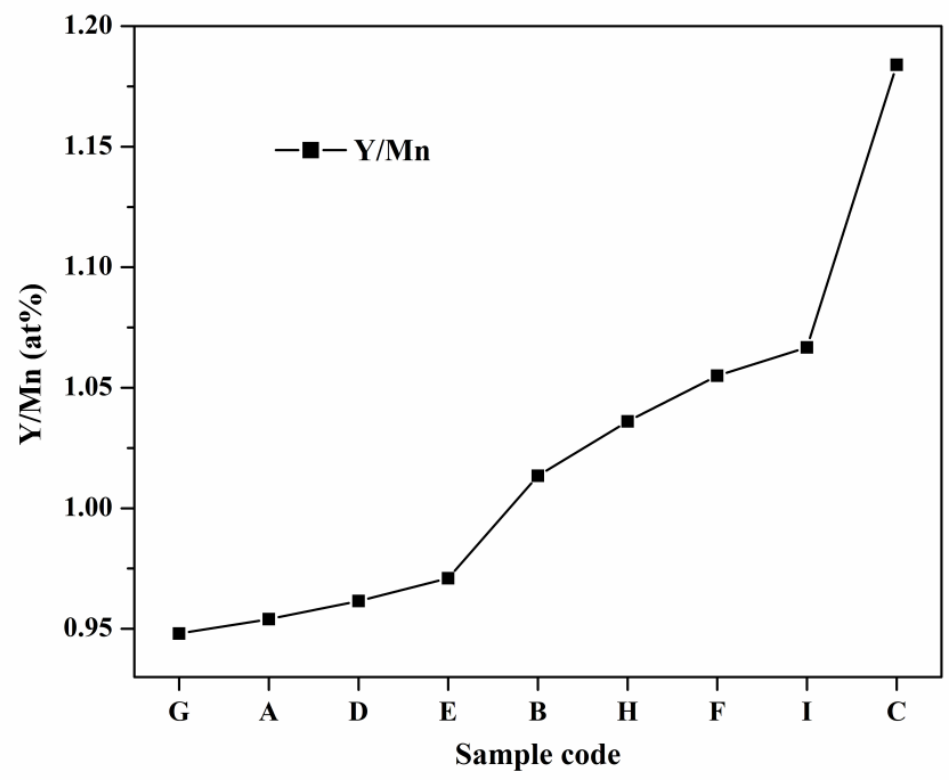

Figure 4.4: Arrangement of samples according to increasing order of Y/Mn ratio

4.2 XRD Analysis

XRD patterns for all samples are shown in Figure 4.5. All the peaks of XRD are matched and indexed with JCPDS, PDF Number 25-1095. All samples show hexagonal crystalline structure with $P6_3cm$ space group **(Wang *et al.* 2011, Raneesh *et al.* 2013**) studied that formation of oxygen vacancy in $RMnO_3$ causes a change in oxidation state of Mn. This affects the bond length of Mn-O and the tolerance factor which correspondingly change the structure. In present case, hexagonal structures of all samples confirm that the oxidation state of Mn is not changed. However, extra peak is observed at 2θ value of ~ 27.76^o in D sample and ~32.40^o in all samples with very small intensity. These peaks are marked by * and correspond to the (220) and (222) planes of Mn_2O_3 respectively **(Sharrouf *et al.*2015, Sharma *et al.* 2016)**. From XRD pattern, Crystallite size (S) was estimated from the most intense peak (112) using Scherrer formula (equation 3.2). Lattice parameter 'a' is calculated from the peak (110) and 'c' is calculated from the peak (004) using the equations 3.4. The exact peak position and Full width at half maxima is calculated from the Gaussian profile fitting for the peaks. Figure

4.6 shows Gauss Cure fitting for (110), (004) and (112) peak with fitting parameters for a representative sample C**.** All the calculated parameters are shown in Table 4.2. All estimated parameters are discussed with respect to change in of Y/Mn ratio and O concentration for the explanation of observed results. Figures 4.7, 4.8, 4.9 and 4.10 respectively show the variation of oxygen concentration (O) as estimated from EDS, and variation of crystallite size (S), lattice parameters 'a' and 'c' with respect to the Y/Mn ratio.

Figure 4.7 shows that O is changing randomly with Y/Mn ratio, and Figure 4.8 shows that crystallite size (S) also seems to behave randomly with change in Y/Mn and Oxygen. Selective samples are need to be discussed to see the effect of cations (Y and Mn) and anion (O) independently. For example, Y/Mn is almost same for samples G (0.948) & A (0.954) but oxygen is not same for them. Crystallite size reduces from sample G to A (while O is increased) i.e. increase in O opposes growth of crystallites and literature **(Tadanaga *et al.* 1998**) show that increase in Y (or Y/Mn) favors crystallization. Both these effects compensate each other, when O and Y/Mn are changing simultaneously. For example, from G to A, S increases due to reduction in O (as Y/Mn is constant), from A to D, S increases due to increase in Y/Mn dominating over increase of O (that wants to reduce S). From sample D to E, increase in Y/Mn is quite small so S does not change much. And from E to B and B to H, increase in Y/Mn dominates and S increases. Now, for samples F, I and C, irrespective of continuous increase in Y/Mn crystallite size changes according to change in O with Y/Mn. So, it can be concluded that Y/Mn ratio is the main deciding factor, for the behavior of S as well as for O to affect S. Effect of O on S changes after Y/Mn exceeds a particular value (1.04). Similar kind of conclusion can be drawn from the variation of 'a' and 'c' with Y/Mn and O (Figures 4.9 and 4.10). Variation of 'a' and 'c' for samples F, I and C follow the trend of change of O w.r.t. to Y/Mn. From literature **(Kitahata *et al.* 1998**) it has been observed that increase in Y/Mn ratio increases both 'a' and 'c' because ionic radius of Y is larger than that of Mn and small change in O does not affect lattice parameters (**Chen *et al.* 2012**). Samples G, B and H are having almost same oxygen conc. (55, 55.3 and 55.3 atm %), but Y/Mn ratio is increasing and so does the value of 'a' and 'c'. Samples D and I also have same 'O' (59.1 and 59.7 atm % respetively) but not Y/Mn ratio. Y/Mn ratio for I is greater than Y/Mn ratio for D and so the value of 'a' and 'c' are larger for I than for D. Significant reduction

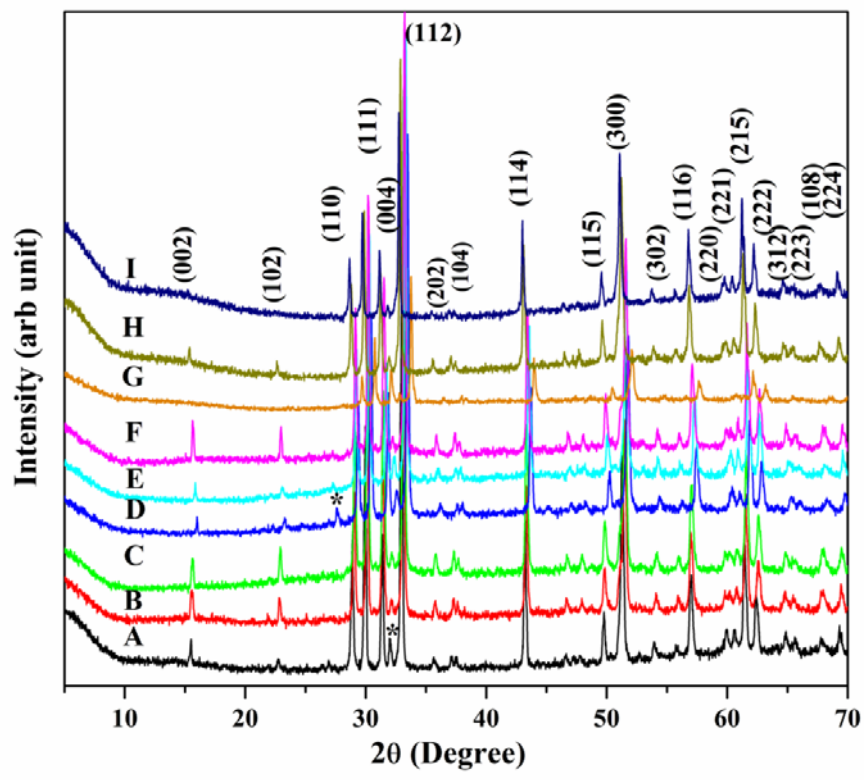

Figure 4.5: XRD pattern for all samples

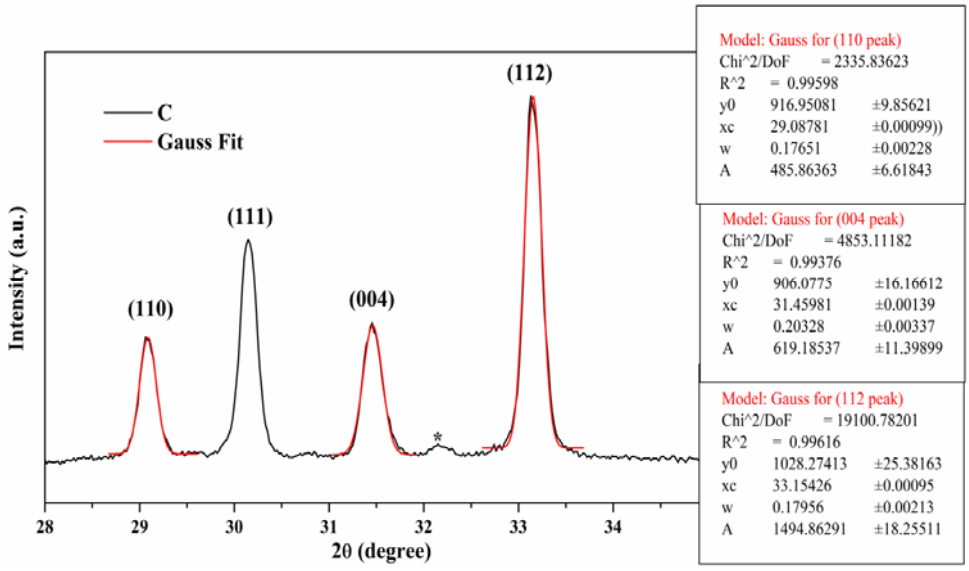

Figure 4.6: Gauss fitting for (110), (112) and (004) peaks for sample C, along with the fitting parameter. Here x_c gives peak position and w full width at half maxima, A area of the peak and y0 is offset.

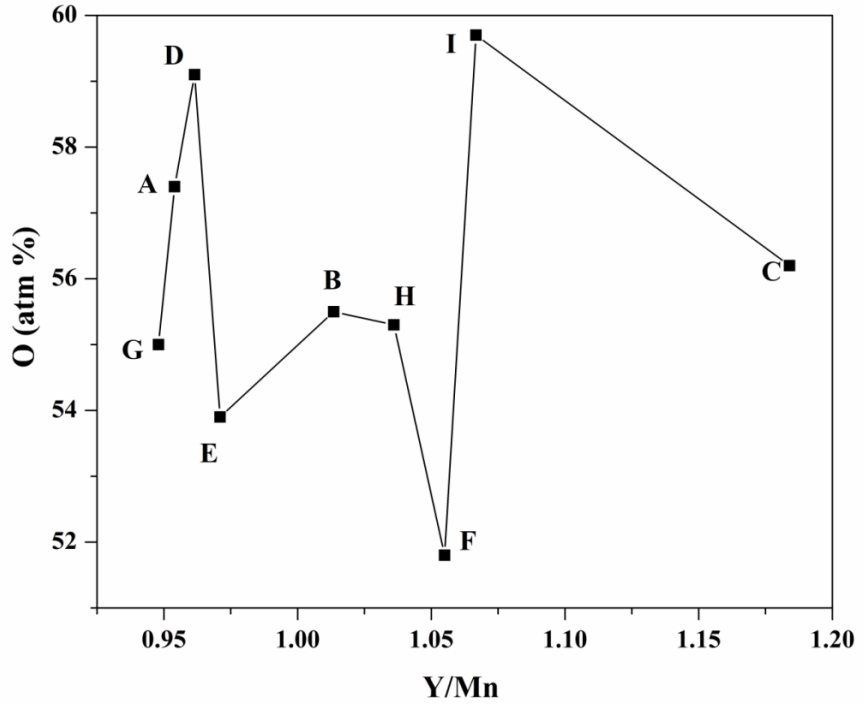

Figure 4.7: Variation of Oxygen conc. (O) with Y/Mn ratio

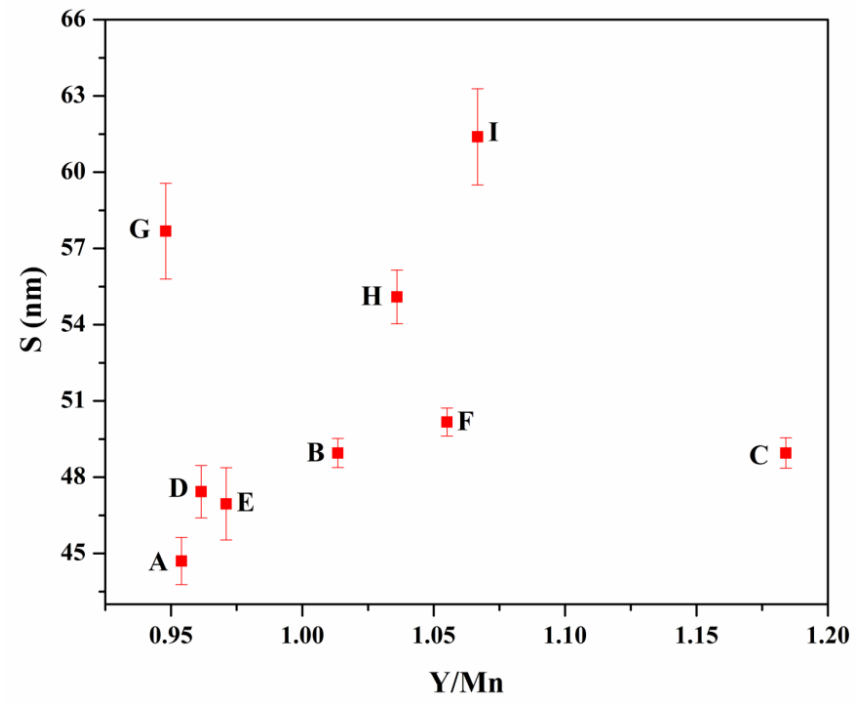

Figure 4.8: Variation of crystallite size (S) with Y/Mn ratio

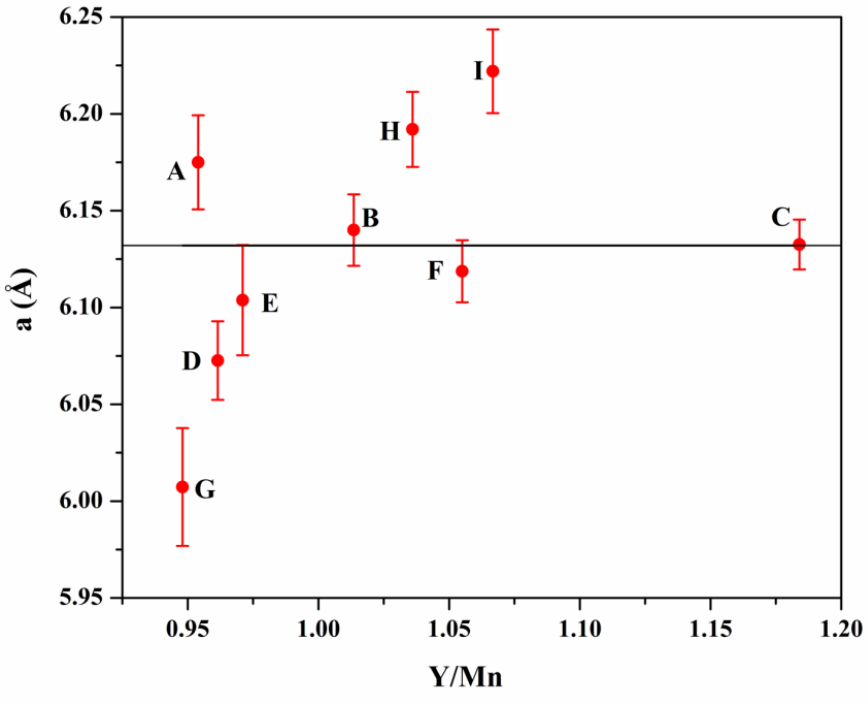

Figure 4.9: Variation of lattice parameters 'a' with Y/Mn ratio. Horizontal Black line is corresponding to a= 6.13Å for stoichiometric $YMnO_3$

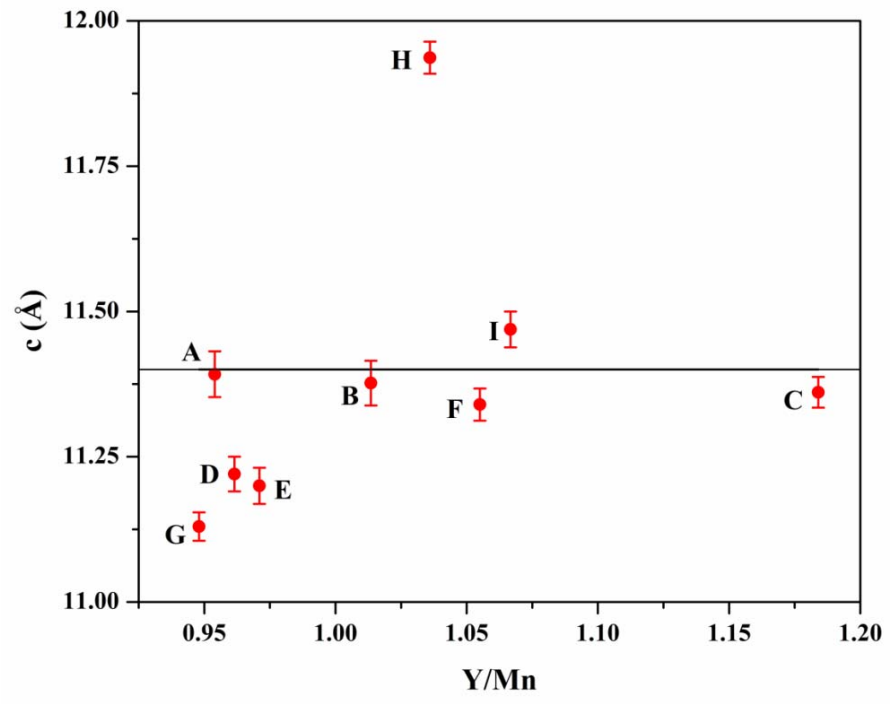

Figure 4.10 : Variation of lattice parameters 'c' with Y/Mn ratio. Horizontal Black line is corresponding to c= 11.4 Å for stoichiometric $YMnO_3$

Table 4.2: Lattice parameters 'a', 'c' and crystallite size 'S' calculated from XRD

Sample codes	Lattice Parameters		Particle Size S (nm)
	a (A^0)	c (A^0)	
A	**6.1750 ± 0.0243**	**11.3920 ± 0.0394**	**44.71 ± 0.93**
B	**6.1400 ± 0.0185**	**11.3767 ± 0.0384**	**48.95 ± 0.57**
C	**6.1325 ± 0.0129**	**11.3610 ± 0.0264**	**47.79 ± 0.60**
D	**6.0726 ± 0.0203**	**11.2202 ± 0.0299**	**47.43 ± 1.03**
E	**6.1038 ± 0.0284**	**11.2700 ± 0.0311**	**46.95 ± 1.42**
F	**6.1187 ± 0.0160**	**11.3398 ± 0.0278**	**50.17 ± 0.55**
G	**6.0073 ± 0.0305**	**11.1299 ± 0.0245**	**57.68 ± 1.88**
H	**6.1919 ± 0.0194**	**11.4366 ± 0.0277**	**55.09 ± 1.06**
I	**6.2222 ± 0.0216**	**11.4691 ± 0.0308**	**69.39 ± 1.88**

in oxygen concentration is found to reduce both 'a' and 'c' remarkably **(Kabbour *et al.* 2017**). Sample F have least oxygen that's why there is decrease in both 'a' and 'c'. It would have least 'a' and 'c' but higher Y/Mn ratio compensates the effect of least O. From sample B to H, increase in 'c' is prominent than increase in 'a' due to increasing Y/Mn ratio (O is almost same). For samples F to I, increase in 'a' is prominent over increase in 'c' due to increasing O (Y/Mn is almost same). Thus it can be concluded that oxygen affects a more than 'c' and Y/Mn affects 'c' more than 'a'. For concentration of Y/Mn > 1 both 'a' and 'c' are close to the values 6.13Å and 11.4Å respectively, as reported for the stoichiometric $YMnO_3$ (**Degenhardt *et al.* 2011, Ahmad *et al.* 2015),** excluding sample I for the case of 'a' and H for both 'a' and 'c'. Since both Y/Mn and O are changing simultaneously from sample to sample hence any regular pattern was not obtained for variation of 'a' and 'c'.

4.3 FTIR Analysis

Figure 4.11 shows the IR spectra of samples A, D, E and F in the range of 490-4500 cm^{-1}. IR spectra give information about the various functional groups and their vibrational modes. Group theory predicts 60 vibrational modes for the space group $P6_3cm$, out of which 25 modes with A_1 and E_1 symmetries are infrared active as well as Raman active. Among rest modes some are Raman active whereas others are inactive

~silent Modes. Figure 4.11 shows broad absorption band in the wavelength range between 4000 and 3000 cm^{-1} which are due to stretching of -OH bond, while sharp peak at around 1643 cm^{-1} is attributed to bending of -OH bond **(Jaganayi *et al.* 2013).** The small intensity peaks in the range from 2300-2360 cm^{-1} are due to C-O bond and overtone of these peaks are appeared in the range of 1100- 1150 cm^{-1} (**Sanati *et al.* 1993)**. Enlarged view of the IR spectra (Figure 4.12) shows that there is a sharp peak at 495 cm^{-1} which is attributed to O-Mn-O bond **(Jaganayi *et al.* 2013, Balamurgan *et al.* 2015).** The small intensity peaks found in the range 510-540 cm^{-1} are attributed to Mn-O stretching vibration mode **(Huang *et al.* 2014, Rahman *et al.* 2015, Kar *et al.* 2015, Peng *et al.* 2017). Djordjevi *et al.* 1965** have also shown that metal-oxygen stretching vibration modes appear in the range from 400-600 cm^{-1}. Presence of Mn_2O_3 peak as shown by XRD is not visible here. The reason for this may be that Mn_2O_3 also has Mn and O so the modes are overlapping with that of $YMnO_3$.

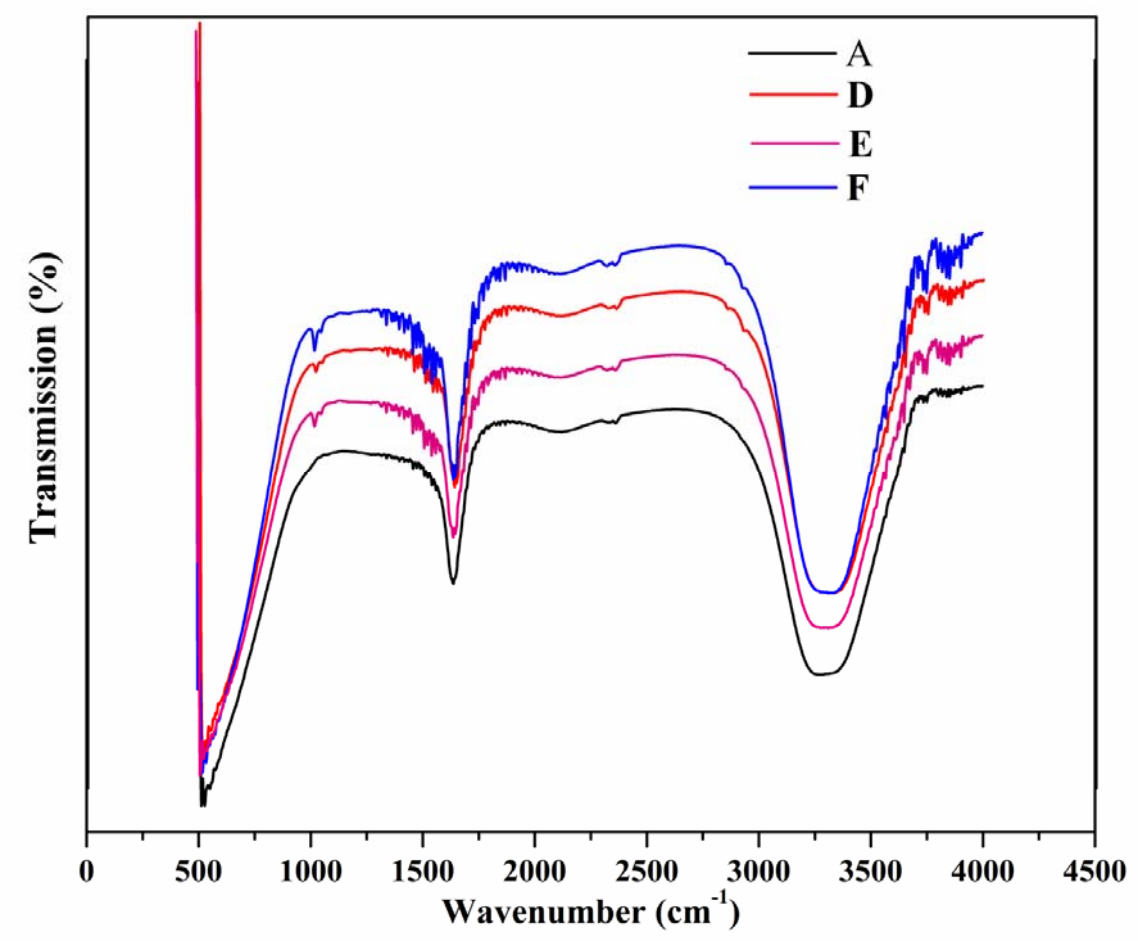

Figure 4.11: IR spectra of samples A, D, E and F in the range of 490- 4500 cm^{-1}

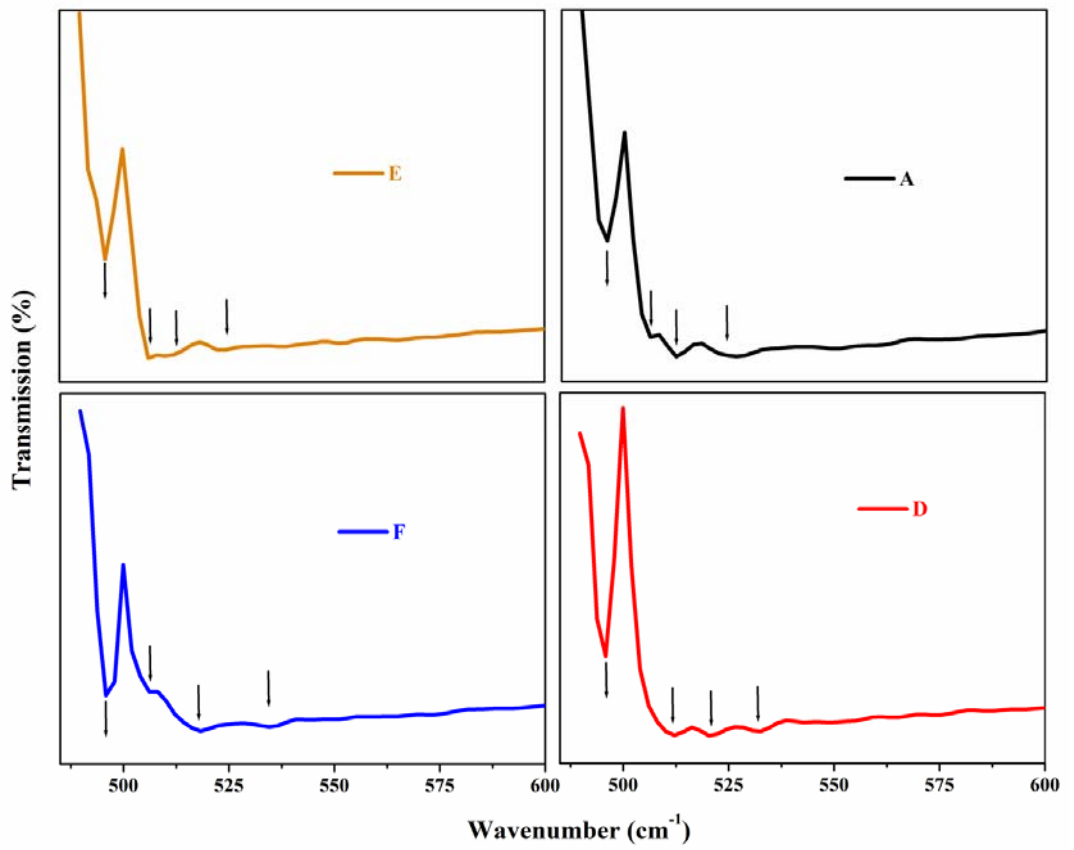

Figure 4.12: Enlarged view of IR spectra of samples A, D, E and F

4.3 Optical Study

UV-Visible spectra recorded in the range of 200-800 nm for all samples are shown in Figure 4.13. The absorption peaks are attributed to the energy band gap of the material. Three Peaks at ~ 1.5 eV, ~ 2.6 eV and ~ 5 eV are observed in absorption spectra of all samples. Figure 4.14 and 4.15 show presence of 3 peaks by Gaussian profile fitting. Peak positions for all samples are listed in Table 4.3. Hexa-$YMnO_3$ has a Mn-O triangular bipyramidal structure and according to Crystal Field Splitting, it has two e_{1g} orbitals (d_{yz} and d_{zx}) at lowest level, followed by two e_{2g} orbitals (d_{xy} and d_{x2-y2}), and one a_{1g} orbital (d_{3z2-r2}). A lay out for these electronic energy levels is shown in Figure 4.16. The first absorption peak at nearly 1.5 eV is attributed to the interband optical transition from the occupied hybridized O 2*p* state with the d_{xy} / d_{x2-y2} orbitals to the unoccupied Mn d_{3z2-r2} state. The second peak at about 2.6 eV is attributed to the interband optical transition from the occupied hybridized O 2*p* state with the d_{yz} /d_{zx} orbitals to the unoccupied Mn d_{3z2-r2} state. The third peak at about 5 eV is the sum of two interband transitions: one from the broad O 2*p* states at ~ −4 eV to the

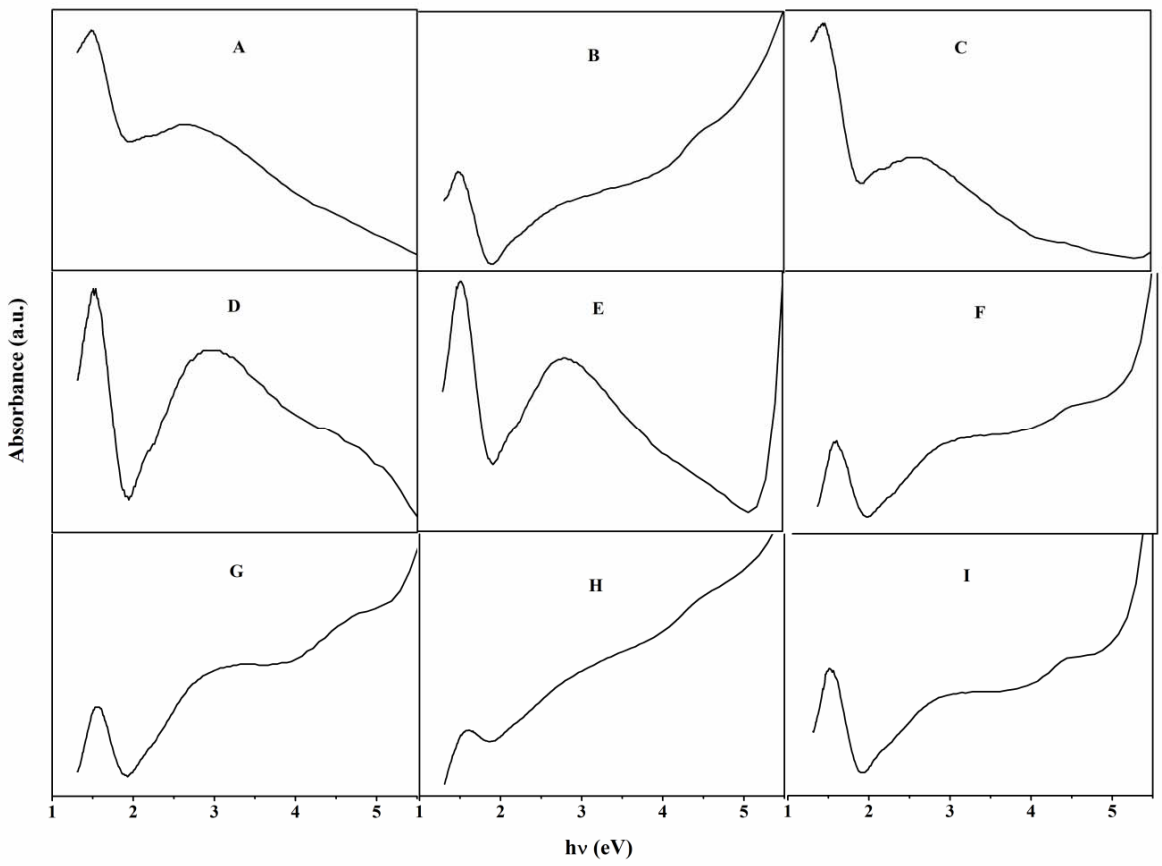

Figure 4.13: UV-Vis spectra for all samples

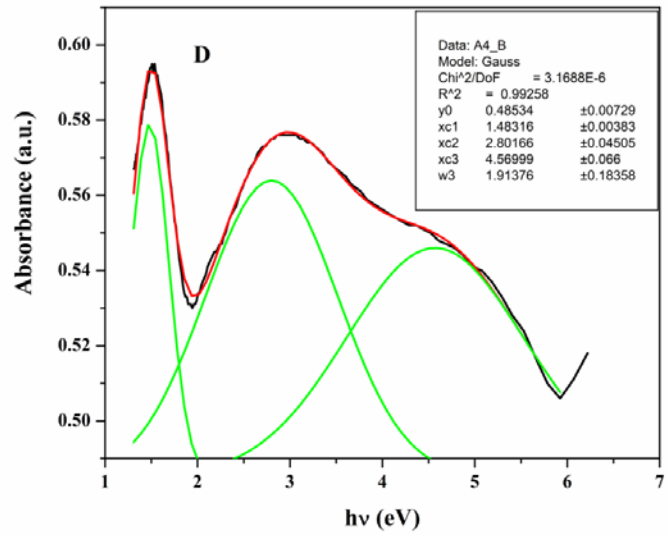

Figure 4.14: Gauss fitting for absorbance vs energy showing 3 peaks for sample D along with fitting parameters. Here x_1, x_{c2}, x_{c3} are peak positions and y0 is offset

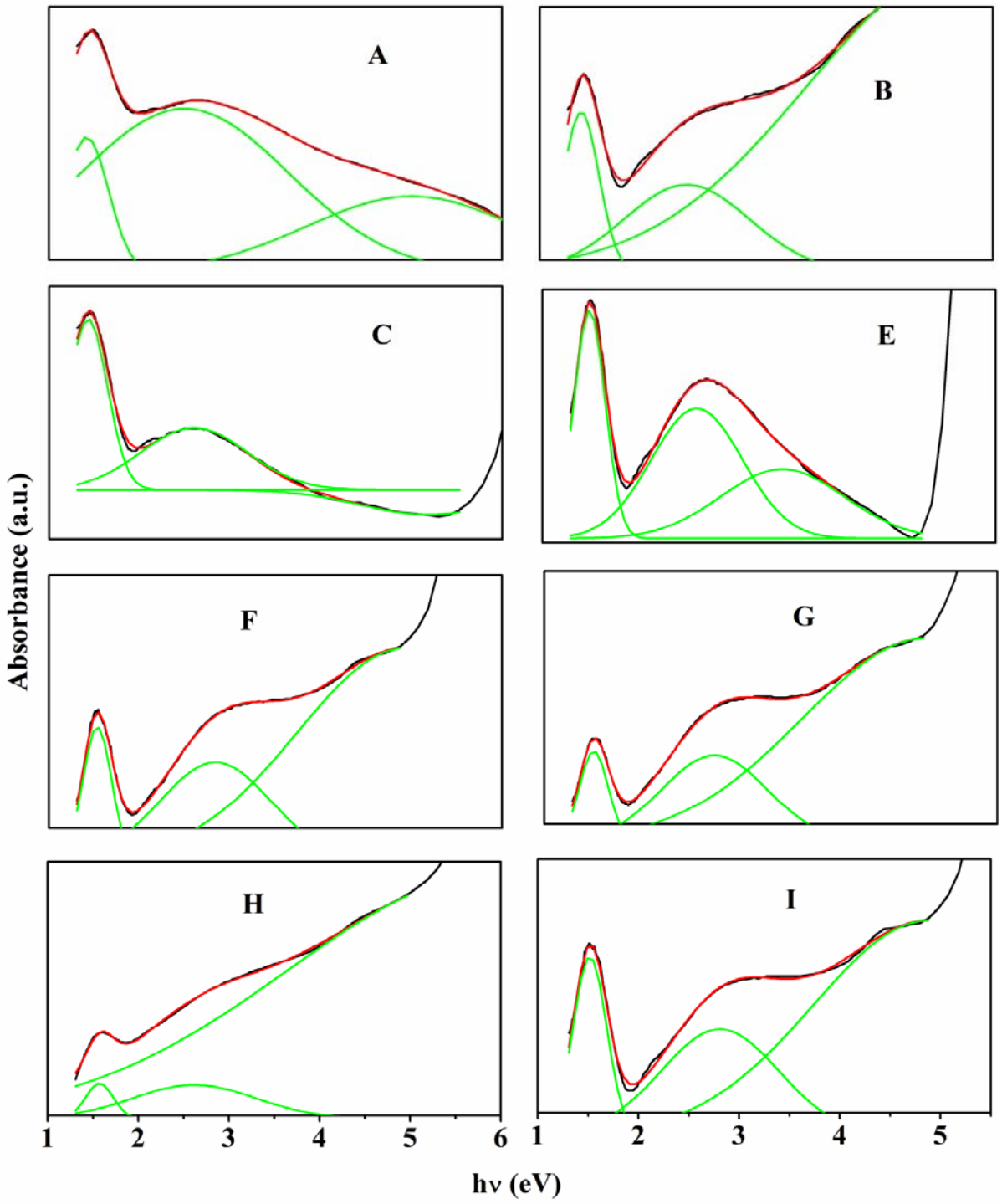

Figure 4.15: Gauss fitting for absorbance vs energy showing 3 peaks for samples A, B, C, E, F, G, H, I

Table 4.3: Peak position for all the samples in UV-Vis spectroscopy.

Sample Code	Eg_1	Eg_2	Eg_3
A	**1.42 ± 0.01**	**2.50 ± 0.14**	**5.00 ± 0.16**
B	**1.46 ± 0.08**	**2.62 ± 0.08**	**5.7 ± 0.01**
C	**1.43 ± 0.01**	**2.60 ± 0.02**	**5.19 ± 0.01**
D	**1.48 ± 0.01**	**2.80 ± 0.05**	**4.57 ± 0.07**
E	**1.52 ± 0.01**	**2.70 ± 0.49**	**3.65 ± 0.22**
F	**1.53 ± 0.01**	**2.84 ± 0.02**	**4.94 ± 0.06**
G	**1.54 ± 0.01**	**2.88 ± 0.01**	**5.23 ± 0.06**
H	**1.54 ± 0.01**	**2.49 ± 0.11**	**5.75 ± 0.34**
I	**1.52 ± 0.01**	**2.81 ± 0.03**	**4.88 ± 0.10**

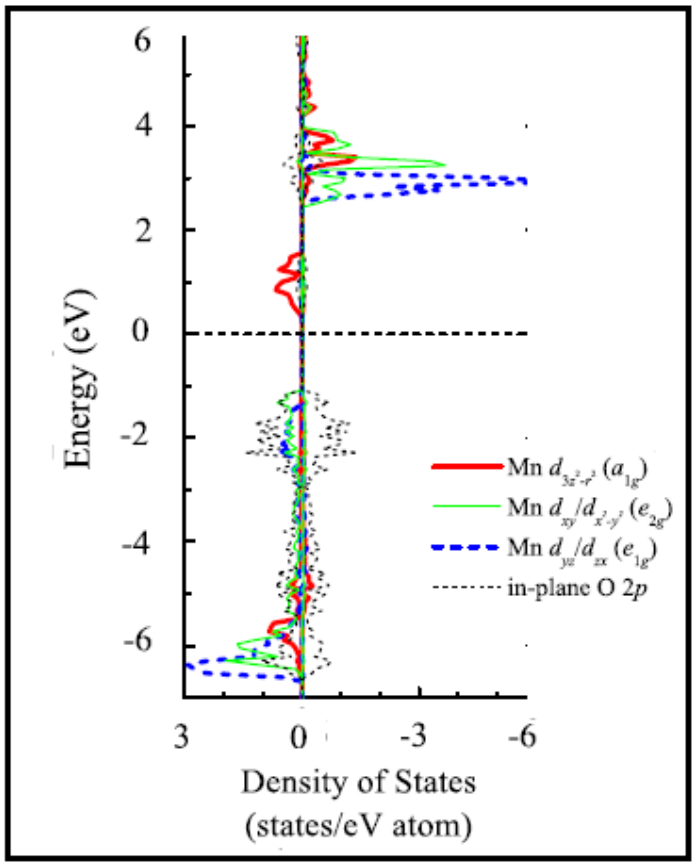

Figure 4.16: Electronic energy levels of $YMnO_3$

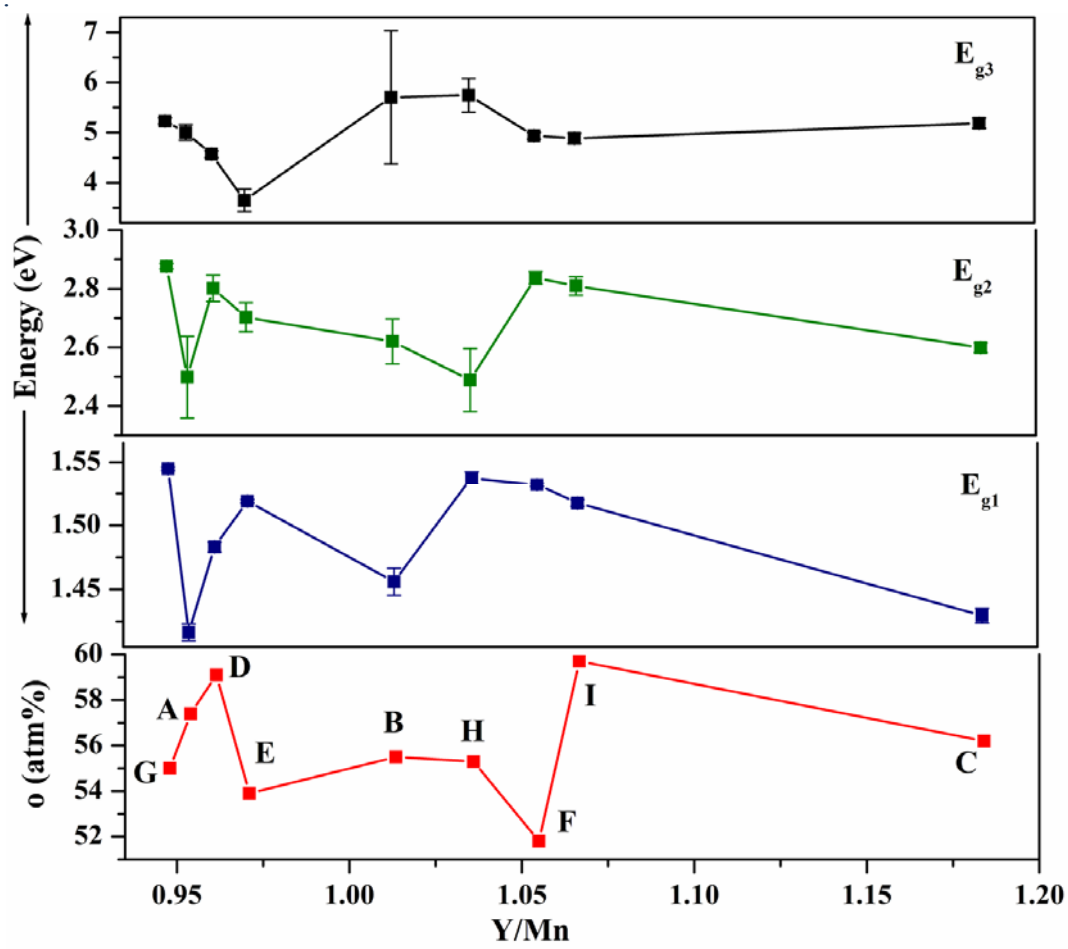

Figure 4.17: Variation of 3 energy gaps and oxygen conc. with Y/Mn ratio

Mn d_{3z2-r2} state, and the other from the O 2p states at ~ −2 eV to the Mn 3*d* states with various orbitals at ~ 3 eV**. (Degenhardt *et al.* 2001, Choi *et al.* 2008).** The peak at around 1.5 eV is important because it is associated with the magnetoelectric coupling in h-$YMnO_3$. **Lima *et al.* 2017** have reported that when non collinear antiferromagnetic interaction is considered between Mn spins, the experimental and theoretical optical spectra match. Figure 4.17 shows the variation of all the three transition energies with Y/Mn ratio. Change in both Y/Mn and O simultaneously, affects the transition energies randomly similar to crystallite size and lattice parameter. However, it seems form the Figure 4.17 that Eg_3 does not vary much with Y/Mn ratio or O conc. After Y/Mn ratio exceeds 1.04 Eg_2 and Eg_1 transition energies reduces (sample F to I and I to C) irrespective of change in O. The transition Eg_1 was found to be more sensitive towards changes in both Y/Mn and O concentration. The transitions corresponding to 2.5 eV and 5eV show that h-YMO behaves as a wide gap semiconductor while the characterstic peak at 1.5 eV indicates its narrow band gap semiconductor type behavior.

Summary and Conclusion

CHAPTER 5 SUMMARY AND CONCLUSION

Multiferroics are special type of materials showing a number of different physical phenomenon that arise due to strong coupling between magnetic, electric and elastic ordering. They have different physical behavior and application in magnetic field sensors, ferromagnetic resonance devices, magnetoelectric memory cells, electro-opto modulator and spin valves etc.

Yttrium magnetite ($YMnO_3$) is an interesting multiferroic material belonging to the hexagonal rare earth magnetite family ($RMnO_3$, R= Trivalent rare earth ion) having $P6_3cm$ space group. This material has potential application in the field of data storage media in non volatile random access memory. Low dielectric constant value of YMO makes this material more useful in device application as it does not suffer from the problem of high electrical noise. It has been seen that the properties of the material can be modified by change in concentration of cations and anions either by substituting different dopant at different sites in $YMnO_3$ or by self doping of Y and Mn. The modified property could have important technological applications. Therefore, present work was focused to study the structural and optical behavior of non-stoichiometric $YMnO_3$.

Synthesis of the sample was done by Solid State reaction method. Structural and optical properties of the prepared non-stoichiometric samples have been investigated by using EDS/SEM, XRD, FTIR, UV-Vis Spectroscopy.

EDS spectra gave information about chemical composition of each sample. No element other than Y, Mn and O were detected in all the samples. Even spite of different stoichiometries, all samples show hexagonal structure, as confirmed by XRD measurement. A small impurity of manganses oxide (Mn_2O_3) is observed in all the samples. It was found that the change in concentrations of Y, Mn and O have different effect on the crystallie size (S) and lattice parameters ‘a’ and ‘c’. Oxygen seems to reduce crystallite size while increasing Y/Mn ratio increases it. After Y/Mn ratio exceeds 1.04, crystallite size behaves similar to that of O with Y/Mn ratio. Y/Mn ratio increases lattice parameters ‘a’ and ‘c’ while O does not affect them much until change in O is significant. If ‘a’ and ‘c’ are compared then O xygen seems to affect ‘a’ and Y/Mn affect ‘c’ more. Simultaneous changes in Y/Mn and O make the behaviour of lattice parameters

and crystallite size random. However, Y/Mn seems to be the main factor to affect structural parameters.

Band positions observed in IR spectra support the XRD results and confirm the presence of hexagonal $YMnO_3$ structure. However, Mn_2O_3 peak as shown by XRD is not visible in the IR spectra because of its Mn-O band position overlapping with that of $YMnO_3$.UV-spectra show three electronic transitions for all samples. These transitions are from occupied hybridized O 2p and Mn 3d states to the unoccupied Mn 3d states. The highest energy ~ 5 eV transition was found to be unaffected by the stoichiometry of the samples. The lowest energy 1.5 eV transition which supports the multiferroic behavior of h-$YMnO_3$ was much affectd by Y/Mn ratio.

Overall it may be concluded, that both Y/Mn and O are important parameters to affect the structural and optical properties of $YMnO_3$. However effect of oxygen changes as Y/Mn ratio exceeds some particular value (usually geater than 1). The effect of variation in Y/Mn and O is compensated with each other to make all parameters behave as observed in results and discussion. More sophisticated experiments are needed to be done for detailed analysis of effect of stoichiometry on physical parameters of $YMnO_3$.

Literature Cited

LITERATURE CITED

Abughayada, C., Dabrowski, B., Kolesnik, S., Brown, D.E. and Chmaissem, O. 2015. Characterization of Oxygen Storage and Structural Properties of Oxygen-Loaded Hexagonal $RMnO_{3+\delta}$ (R= Ho, Er, and Y). *Chemistry of Materials*, 27(18): 6259-6267.

Ahmad, T., Lone, I.H. and Ubaidullah, M. 2015. Structural characterization and multiferroic properties of hexagonal nano-sized $YMnO_3$ developed by a low temperature precursor route**.** *RSC Advances*, 5(71): 58065-58071.

Asaka, T., Nemoto, K., Kimoto, K., Arima, T. and Matsui, Y. 2005. Crystallographic superstructure of Ti-doped hexagonal $YMnO_3$. *Physical Review B*, 71(1):014114.

Balamurugan, C., & Lee, D. W. 2015. Perovskite hexagonal $YMnO_3$ nanopowder as p-type semiconductor gas sensor for H_2S detection. *Sensors and Actuators B: Chemical,* 221: 857-866.

Chauhan, S., Srivastava, S.K., Rajput, A.S. and Chandra, R. 2014. Effect of Gd-substitution at Y-site on the structural, magnetic and dielectric properties of $Y_{1-x}Gd_xMnO_3$ (x= 0, 0.05) nanoparticles. *MRS Online Proceedings Library Archive,* 1675*:*121-128.

Chen, D.P., Du, Y., Wang, X.L., Cheng, Z.X., Dou, S.X., Lin, Z.W., Zhu, J.G. and Xu, B. 2012. Oxygen-vacancy effect on structural, magnetic, and ferroelectric properties in multiferroic $YMnO_3$ single crystals. *Journal of Applied Physics*, 111(7): 07D913.

Cheng, S., Deng, S.Q., Zhao, Y.G., Sun, X.F. and Zhu, J. 2015. Correlation between oxygen vacancies and sites of Mn ions in $YMnO_3$. *Applied Physics Letters*, 106(6): 062905.

Cheng, S., Li, M., Deng, S., Bao, S., Tang, P., Duan, W., & Zhu, J. 2016. Manipulation of magnetic properties by oxygen vacancies in multiferroic $YMnO_3$. *Advanced Functional Materials*, 26(21): 3589-3598.

Choi, W.S., Kim, D.G., Seo, S.S.A., Moon, S.J., Lee, D., Lee, J.H., Lee, H.S., Cho, D.Y., Lee, Y.S., Murugavel, P. and Yu, J. 2008. Electronic structures of hexagonal $RMnO_3$ (R= Gd, Tb, Dy, and Ho) thin films: Optical spectroscopy and first-principles calculations. *Physical Review B*, 77(4): 045137.

Dabrowski, B., Remsen, S., Mais, J. and Kolesnik, S. 2011. Synthesis amd characterization of Non-stoichiometric hexagonal $Dy_{1-x}Y_xMnO_{3+\delta}$. *Functional Materials Letters*, 4(02): 147-150.

Dai, Y., Zhang, A.M., Yang, L.P., Gao, Z.R. and Wu, X.S. 2016. Investigation of structure and magnetic properties of Ru-doped $YMnO_3$. *Journal of Applied Physics*, 120(4): 04410.

Degenhardt, C., Fiebig, M., Fröhlich, D., Lottermoser, T., & Pisarev, R. V. 2001. Nonlinear optical spectroscopy of electronic transitions in hexagonal manganites. *Applied Physics B,* 73(2): 139-144.

Djordjevic, C. 1965. Metal-Oxygen Stretching frequencies in some γ-nitroacetylacetonates in solids and solution infra red spectra. *Acta Spectrochimica,* 21: 1018-1020

Dixit, G., Singh, J.P., Chen, C.L., Dong, C.L., Srivastava, R.C., Agrawal, H.M., Pong, W.F. and Asokan, K. 2013. Study of structural, morphological and electrical properties of Ce doped NiFe2O4 nanoparticles and their electronic structure investigation. *Journal of Alloys and Compounds*, 581:178-185.

Du, Y., Wang, X.L., Chen, D.P., Dou, S.X., Cheng, Z.X., Higgins, M., Wallace, G. and Wang, J.Y. 2011. Domain wall conductivity in oxygen deficient multiferroic $YMnO_3$ single crystals. *Applied Physics Letters*, 99(25): 252107.

Eerenstein, W., Mathur, N.D. and Scott, J.F. 2006. Multiferroic and magnetoelectric materials**.** *Nature*, 442(7104): 759.

Fennie, C.,Rabe, K.M.,2005. Ferroelectric transition in$YMnO_3$ from first principles. *Physical Review B* 72: 100103–100104.

Fiebig, M.,Lottermoser,Th.,Fröhlich,D.,Goltsev,A.V.,Pisarev,R.V.,2002.Observation of coupled magnetic and electric domains**.** *Nature* 419*:* 818–820.

Gelard, I., Jehanathan, N., Roussel, H., Gariglio, S., Lebedev, O.I., Van Tendeloo, G. and Dubourdieu, C. 2011. Off-stoichiometry effects on the crystalline and defect structure of hexagonal manganite $REMnO_3$ films (RE= Y, Er, Dy). *Chemistry of Materials*, *23*(5): 1232-1238.

Gibbs, A.S., Knight, K.S. and Lightfoot, P. 2011. High-temperature phase transitions of hexagonal $YMnO_3$. *Physical Review B*, 83(9): 094111.

Gelard, I., Jehanathan, N., Roussel, H., Gariglio, S., Lebedev, O.I., Van Tendeloo, G. and Dubourdieu, C. 2011. Off-stoichiometry effects on the crystalline and defect structure of hexagonal manganite $REMnO_3$ films (RE= Y, Er, Dy). *Chemistry of Materials*, 23(5): 1232-1238.

Schmid, H. 1994. Multi-ferroic magnetoelectrics. *Ferroelectrics*, 162(1):317-338.

Han, A., Zhao, M., Ye, M., Liao, J., Zhang, Z. and Li, N. 2013. Crystal structure and optical properties of $YMnO_3$ compound with high near-infrared reflectance. *Solar Energy*, 91: 32-36.

Helmolt, R., Wecker, J., Holzapfel, B., Schultz, L. and Samwer, K. 1993. Giant negative magnetoresistance in perovskitelike $La_{2/3}Ba_{1/3}MnO_x$ ferromagnetic films. *Physical Review Letters*, 71(14): 2331.

Huang, Z. J., Cao, Y., Sun, Y. Y., Xue, Y. Y., & Chu, C. W. (1997). Coupling between the ferroelectric and antiferromagnetic orders in $YMnO_3$. *Physical Review B*, 56(5): 2623.

Huang, M., Zhang, Y., Li, F., Zhang, L., Ruoff, R.S., Wen, Z. and Liu, Q. 2014. Self-assembly of mesoporous nanotubes assembled from interwoven ultrathin birnessite-type MnO_2 nanosheets for asymmetric supercapacitors. *Scientific reports*, 4: 3878.

Jaganyi, D., Altaf, M. and Wekesa, I. 2013. Synthesis and characterization of whisker-shaped MnO_2 nanostructure at room temperature. *Applied Nanoscience*, 3(4): 329-333.

Jin, S., Tiefel, T.H., McCormack, M., Fastnacht, R.A., Ramesh, R. and Chen, L.H. 1994. Thousandfold change in resistivity in magnetoresistive La-Ca-Mn-O films. *Science*, 264(5157): 413-415.

Kabbour, H., Gauthier, G.H., Tessier, F., Huvé, M., Pussacq, T., Roussel, P., Hayward, M.A., Moreno B, Z.L., Marinova, M., Colmont, M. and Colis, S. 2017. Topochemical Reduction of $YMnO_3$ into a Composite Structure. *Inorganic chemistry*, 56(14): 8547-8553.

Kalashnikova, A.M. and Pisarev, R.V. 2003. Electronic structure of hexagonal rare-earth manganites $RMnO_3$. *Journal of Experimental and Theoretical Physics Letters*, 78(3): 143-147.

Kang, J.S., Han, S.W., Park, J.G., Wi, S.C., Lee, S.S., Kim, G., Song, H.J., Shin, H.J., Jo, W. and Min, B.I. 2005. Photoemission and x-ray absorption of the electronic structure of multiferroic $RMnO_3$ (R= Y, Er). *Physical Review B*, 71(9): 092405.

Kar, P., Sardar, S., Ghosh, S., Parida, M.R., Liu, B., Mohammed, O.F., Lemmens, P. and Pal, S.K. 2015. Nano surface engineering of Mn_2O_3 for potential light-harvesting application. *Journal of Materials Chemistry C*, 3(31): 8200-8211.

Khomskii, D. (2009). Trend: Classifying multiferroics: Mechanisms and effects. *Physics*, 2: 20.

Kim, S.H., Lee, S.H., Kim, T.H., Zyung, T., Jeong, Y.H. and Jang, M.S. 2000. Growth**,** ferroelectric properties, and phonon modes of $YMnO_3$ single crystal. *Crystal Research and Technology: Journal of Experimental and Industrial Crystallography*, 35(1): 19-27.

Kimura, T., Kawamoto, S., Yamada, I., Azuma, M., Takano, M. and Tokura, Y. 2003. Magnetocapacitance effect in multiferroic BiMnO 3. *Physical Review B*, 67(18): 180401.

Kitahata, H., Tadanaga, K., Minami, T., Fujimura, N. and Ito, T. 1998. Microstructure and Dielectric Properties of $YMnO_3$ Thin Films Prepared by Dip□Coating. *Journal of the American Ceramic Society*, 81(5): 1357-1360.

Lima, A. F., & Lalic, M. V. 2017. Optical absorption spectrum and electronic structure of multiferroic hexagonal $YMnO_3$ compound. *Optical Materials*, 64: 406-412.

Makhdoom, A. R., Akhtar, M. J., Rafiq, M. A., & Hassan, M. M. 2012. Investigation of transport behavior in Ba doped $BiFeO_3$. *Ceramics International*, 38(5): 3829-3834.

Martin, L.W., Crane, S.P., Chu, Y.H., Holcomb, M.B., Gajek, M., Huijben, M., Yang, C.H., Balke, N. and Ramesh, R. 2008. Multiferroics and magnetoelectrics: thin films and nanostructures. *Journal of Physics: Condensed Matter*, 20(43): 434220.

Mori, S., Tokunaga, J., Horibe, Y., Aikawa, Y. and Katsufuji, T. 2005. Magnetocapacitance effect and related microstrucuture in Ti-doped $YMnO_3$. *Physical Review B*, 72(22): 224434.

Muneeswaran, M., Jang, J. W., Choi, B. C., Jeong, J. H., & Giridharan, N. V. 2017. Structural, optical and multiferroic properties of pure and Dy modified $YMnO_3$. *Journal of Materials Science: Materials in Electronics*, 28(22): 16788-16796.

Peng, F.F., Jin, M.M., Long, C.Y., Tang, P.S. and Chen, H.F. 2017. Preparation and Characterization of $YMnO_3$ by Microwave Assisted Process. In *Key Engineering Materials* 748: 428-432.

Rahaman, H., Laha, R.M., Maiti, D.K. and Ghosh, S.K. 2015. Fabrication of Mn_2O_3 nanorods: an efficient catalyst for selective transformation of alcohols to aldehydes**.** *RSC Advances*, 5(43): 33923-33929.

Rathod, K.N., Rajyaguru, B., Solanki, S., Shrimali, V.G., Sagapariya, K., Markna, J.H., Solanki, P.S. and Shah, N.A. 2016. Studies on structural and electrical properties of pure and doped h-$YMnO_3$. In *AIP Conference Proceedings* 1728(1): 020527.

Raneesh, B., Saha, A., & Kalarikkal, N. 2013. Effect of gamma radiation on the structural, dielectric and magnetoelectric properties of nanostructured hexagonal $YMnO_3$**.** *Radiation Physics and Chemistry*, 89: 28-32.

Sanati, M. and Andersson, A. 1993. DRIFT study of the oxidation and the ammoxidation of toluene over a TiO_2 (B)-supported vanadia catalyst. *Journal of molecular catalysis*, 81(1): 51-62.

Sharma, S., Chauhan, P., & Husain, S. 2016. Structural and optical properties of Mn_2O_3 nanoparticles & its gas sensing applications. *Advanced Materials Proceedings,* 1(2*):* 220-225

Sharrouf, M., Awad, R., Roumié, M., & Marhaba, S. 2015. Structural, Optical and Room Temperature Magnetic Study of Mn_2O_3 Nanoparticles. *Materials Sciences and Applications*, 6(10): 850.

Sekhar, M.C., Padmavathi, K., Park, J.G. and Venugopal Reddy, P. 2003. Elastic Behavior of $YMnO_3$ and $ErMnO_3$ Manganites. *Modern Physics Letters B*, 17(20n21): 1119-1125.

Smolenskii, G.A. and Bokov, V.A. 1964. Coexistence of magnetic and electric ordering in crystals. *Journal of Applied Physics*, 35(3): 915-918.

Tadanaga, K., Kitahata, H., Minami, T., Fujimura, N. and Ito, T. 1998. Preparation and Dielectric Properties of $YMnO_3$ Ferroelectric Thin Films by the Sol-Gel Method. *Journal of sol-gel science and technology*, 13(1-3): 903-908.

Uniyal, P. and Yadav, K.L. 2008. Study of dielectric, magnetic and ferroelectric properties in $Bi_{1-x}Gd_xFeO_3$. *Materials Letters*, 62(17-18): 2858-2861.

Vajk, O.P., Kenzelmann, M., Lynn, J.W., Kim, S.B., Cheong, S.W. 2005. Magneticorder and spin dynamics in ferroelectric $HoMnO_3$. *Physical Review Letters* 94: 087601–087604.

Van Aken, B. B., Palstra, T. T., Filippetti, A., & Spaldin, N. A. 2004. The origin of ferroelectricity in magnetoelectric $YMnO_3$. *Nature materials*, 3(3): 164.

Wang, J. B. N. J., Neaton, J. B., Zheng, H., Nagarajan, V., Ogale, S. B., Liu, B. & Spaldin, N. A. 2003. Epitaxial $BiFeO_3$ multiferroic thin film heterostructures. S*cience*, 299(5613), 1719-1722.

Wang, S.F., Yang, H., Xian, T. and Liu, X.Q. 2011. Size-controlled synthesis and photocatalytic properties of $YMnO_3$ nanoparticles**.** *Catalysis Communications*, 12(7): 625-628.

Yakel, H. L., Koehler, W. C., Bertaut, E. F., & Forrat, E. F. 1963. On the crystal structure of the manganese (III) trioxides of the heavy lanthanides and yttrium. *Acta Crystallographica*, 16(10): 957-962.

Yoo, Y.J., Lee, Y.P., Park, J.S., Kang, J.H., Kim, J., Lee, B.W. and Seo, M.S. 2012. Spin-glass behavior of Cr-doped $YMnO_3$ compounds. *Journal of Applied Physics*, 112(1): 013903.

Zhang, A.M., Zhu, W.H., Wu, X.S. and Bian, Q. 2013. Spin-frustrated effect and the magnetic properties in $YMn_{1-x}Al_xO_3$. *Modern Physics Letters B*, 27(22): 1350163.

VITA

Priya Mehra, the authoress of this manuscript, was born on 29thAugust, 1995 at Ramnagar (Nainital), Uttarakhand. She successfully completed her high school and intermediate in the year 2011 and 2013, respectively from M.P.H. Inter College, Ramnagar. Thereafter, she joined P.N.G.P.G. College, Ramnagar (Kumaun University) for graduation and passed her B.Sc. degree in the year 2016. Subsequently the authoress joined College of Basic Science and Humanities, Govind Ballabh Pant University of Agriculture & Technology, Pantnagar, Uttarakhand, for the degree of M.Sc. in Physics.

Address of Correspondence:

Priya Mehra
D/o- Mrs. Sarita Mehra & Mr. I.S. Mehra
Bharatpuri, Ramnagar
Pin- 244715
Distt- Nainital
Uttarakhand
E-mail: mehrapriya0829@gmail.com

ABSTRACT

Name : Priya Mehra **Id. No.** : 51095

Year of admission : 2016-2017 **Degree** : M.Sc.

Dept. : Physics

Major : Physics

Thesis Title : "Study of Structural and Optical Behaviour of Non-Stoichiometric Hexagonal $YMnO_3$"

Advisor : Dr. Gagan Dixit

In the present work, structural and optical properties of non-stoichiometric hexagonal $YMnO_3$ have been studied. Physical properties mainly structural, electrical and magnetic were found to be modified by doping of elements at Y or Mn sites in $YMnO_3$ and by oxygen vacancies or excess oxygen. This provides motivation to study the effect of different concentrations of Y, Mn or O on the structural and optical properties of the non-stoichiometric $YMnO_3$ samples. The synthesis of the sample was done by Solid State reaction method. The samples were characterized by using EDS/SEM, XRD, FTIR and UV-Vis Spectroscopy. EDS spectra gave information about chemical composition of each sample. XRD pattern and IR spectra confirmed the hexagonal structure of all the non stoichiometric samples. However, a small impurity of Mn_2O_3 was observed in all the samples. Absorbance spectra obtained by UV-Vis spectroscopy informed about different electronic energy levels of the samples. Three absorption peaks were found in all samples corresponding to three electronic transitions from occupied hybridized (O 2*p* and Mn 3d) states to the unoccupied Mn 3d states. All results were discussed in terms of Y/Mn ratio and O concentration. It was found that simultaneous changes in concentrations of Y, Mn and O affect particle size (S), lattice parameters 'a' and 'c' and electronic transitions in random ways. Increase in Y/Mn ratio was found to increase 'S', 'a' and 'c' with constant O. Effect of oxygen concentration was different depending upon Y/Mn exceeds 1 or is less than 1. The energy of electronic levels changes with stoichiometry of the composition though this change is not uniform for all the levels.

(Gagan Dixit)
Advisor

(Priya Mehra)
Authoress

सारांश

नाम	: प्रिया मेहरा	**परिचयांक**	: ५१०९५
सत्र एवम् प्रवेश वर्ष	I/२०१६-१७	**उपाधि**	: स्नातकोत्तर
प्रमुख	: भौतिकी	**विभाग**	: भौतिक विज्ञान
शोध ग्रन्थ शीर्षक	: "नॉन स्टॉइकियोमिट्रिक हेक्सागोनल $YMnO_3$ के संरचनात्मक एवं ऑप्टिकल व्यवहार का अध्ययन "		
सलाहकार	: डॉ गगन दीक्षित		

वर्तमान कार्य में नॉन स्टॉइकियोमिट्रिक हेक्सागोनल $YMnO_3$ के संरचनात्मक एवं ऑप्टिकल व्यवहार का अध्ययन किया गया । पुराने शोध परिणामों से Y या Mn साइटों पर डोपिंग तथा ऑक्सीजन की अधिकता या रिक्तियों द्वारा भौतिक गुणधर्म मुख्यतः संरचनात्मक, विद्युतीय एवं चुंबकीय गुणों में परिवर्तन पाया गया है। इन्हीं परिवर्तनों के फलस्वरूप हमें नॉन स्टॉइकियोमिट्रिक $YMnO_3$ में Y, Mn और O के विभिन्न सांद्रता वाले यौगिकों की संरचनात्मकता एवं ऑप्टिकल व्यवहार का अध्ययन करने प्रेरणा मिली । यौगिकों का संश्लेषण ठोस अवस्था अभिक्रिया विधि द्वारा किया गया । यौगिकों का निरुपण EDS/SEM, XRD, FTIR और UV-Vis स्पेक्ट्रोस्कोपी द्वारा किया गया । रासायनिक संरचना का विश्लेषण EDS स्पेक्ट्रा द्वारा किया गया । नॉन स्टॉइकियोमिट्रिक यौगिकों की हेक्सागोनल संरचना की पुष्टि XRD एवं IR स्पेक्ट्रा द्वारा की गयी । सभी यौगिकों में Mn_2O_3 की लघु अशुद्धि पायी गयी । UV-Vis स्पेक्ट्रोस्कोपी से प्राप्त अवशोषण वर्णक्रम द्वारा इलेक्ट्रॉनिक ऊर्जा स्तरों की जानकारी प्राप्त हुई । सभी यौगिकों में O $2p$ तथा Mn 3d के भृत संकरण से अभृत Mn 3d कक्षक में इलेक्ट्रोनिक संक्रांति के अनुरूप तीन अवशोषण श्रृंग प्राप्त हुए । सभी यौगिकों के परिणामों की चर्चा Y/Mn के अनुपात एवं ऑक्सीजन की सांद्रता के अनुरूप की गयी । यह पाया गया की Y, Mn और O की सांद्रता का साथ साथ परिवर्तित होना कणों के आकार (S), लैटिस पैरामीटर 'a' और 'c' तथा इलेक्ट्रोनिक संक्रांति को अनियमित रूप से प्रभावित करता है । O के सतत रहने पर Y/Mn अनुपात में वृद्धि के अनुरूप ही कणों के आकार (S) एवं लैटिस पैरामीटर 'a' और 'c' में वृद्धि पायी गयी । O की सांद्रता Y/Mn अनुपात के 1 या 1 से कम पर विभिन्न प्रकार से प्रभाव डालती है । यह भी पाया गया कि इलेक्ट्रॉनिक ऊर्जा स्तरों की ऊर्जा, यौगिक की स्टॉइकियोमिट्रि से प्रभावित होती है, हालांकि यह प्रभाव सभी ऊर्जा स्तरों के लिये अलग अलग है ।

Gagan Dixit

(गगन दीक्षित)
सलाहकार

Priya Mehra

(प्रिया मेहरा)
लेखिका